A Section 508–conformant HTML version of this article is available at https://doi.org/10.1289/EHP9256.

Evaluation of Placentation and the Role of the Aryl Hydrocarbon Receptor Pathway in a Rat Model of Dioxin Exposure

Khursheed Iqbal,[1,2] *Stephen H. Pierce,*[1,2,*] *Keisuke Kozai,*[1,2] *Pramod Dhakal,*[1,2,†] *Regan L. Scott,*[1,2] *Katherine F. Roby,*[1,3] *Carrie A. Vyhlidal,*[1,4,5,6] *and Michael J. Soares*[1,2,5,7]

[1]Institute for Reproduction and Perinatal Research, University of Kansas Medical Center (KUMC), Kansas City, Kansas, USA
[2]Department of Pathology and Laboratory Medicine, KUMC, Kansas City, Kansas, USA
[3]Department of Anatomy and Cell Biology, KUMC, Kansas City, Kansas, USA
[4]Division of Clinical Pharmacology, Toxicology and Therapeutic Innovation, Children's Mercy Kansas City, Kansas City, Missouri
[5]Center for Perinatal Research, Children's Mercy Research Institute, Children's Mercy Kansas City, Kansas City, Missouri
[6]Department of Pediatrics, University of Missouri-Kansas City School of Medicine, Kansas City, Missouri
[7]Department of Obstetrics and Gynecology, KUMC, Kansas City, Kansas, USA

Background: Our environment is replete with chemicals that can affect embryonic and extraembryonic development. Dioxins, such as 2,3,7,8-tetrachlorodibenzo-*p*-dioxin (TCDD), are compounds affecting development through the aryl hydrocarbon receptor (AHR).

Objectives: The purpose of this investigation was to examine the effects of TCDD exposure on pregnancy and placentation and to evaluate roles for AHR and cytochrome P450 1A1 (CYP1A1) in TCDD action.

Methods: Actions of TCDD were examined in wild-type and genome-edited rat models. Placenta phenotyping was assessed using morphological, biochemical, and molecular analyses.

Results: TCDD exposures were shown to result in placental adaptations and at higher doses, pregnancy termination. Deep intrauterine endovascular trophoblast cell invasion was a prominent placentation site adaptation to TCDD. TCDD-mediated placental adaptations were dependent upon maternal AHR signaling but not upon placental or fetal AHR signaling nor the presence of a prominent AHR target, CYP1A1. At the placentation site, TCDD activated AHR signaling within endothelial cells but not trophoblast cells. Immune and trophoblast cell behaviors at the uterine–placental interface were guided by the actions of TCDD on endothelial cells.

Discussion: We identified an AHR regulatory pathway in rats activated by dioxin affecting uterine and trophoblast cell dynamics and the formation of the hemochorial placenta. https://doi.org/10.1289/EHP9256

Introduction

Hemochorial placentation, as seen in the human, rat, and mouse involves lineage-specific development of specialized trophoblast cell types, which orchestrate the efficient redirection of blood flow to the placenta and delivery of nutrients to the fetus (Georgiades et al. 2002; Knöfler et al. 2019; Maltepe and Fisher 2015; Soares et al. 2018). Pregnancy-related diseases such as preeclampsia, intrauterine growth restriction, and preterm birth are associated with dysfunctional placentation, especially failures in endovascular trophoblast cell invasion and uterine spiral artery remodeling (Brosens et al. 2011, 2019). The rat exhibits deep intrauterine trophoblast cell invasion resembling human placentation and is a useful model for investigating regulatory events at the maternal–fetal interface (Pijnenborg and Vercruysse 2010; Soares et al. 2012).

Placental plasticity is a key to a successful pregnancy (Soares et al. 2014, 2018). The placenta can adapt structurally and functionally to environmental challenges, ensuring nutrient and gas exchange and permitting fetal development to proceed. However, these adaptive mechanisms can be overwhelmed or disrupted leading to altered fetal nutrient and gas supply, which is detrimental to fetal growth and maturation (Sferruzzi-Perri and Camm 2016; Vaughan et al. 2011). *In utero* insults affecting placentation can result in lifelong health consequences (Burton et al. 2016). Differences between healthy and diseased states can be attributed to the effectiveness of placenta-dependent adaptations to environmental challenges (Soares et al. 2014, 2018). Molecular mechanisms underlying placental adaptations to environmental exposures are poorly understood.

Endocrine disruptors are a class of environmental exposures that act to interfere with normal cell signaling pathways (Gore et al. 2015). Some endocrine disruptors are ubiquitous in our environment and represent a significant public health concern (Bergman et al. 2013; Gore et al. 2015; La Merrill et al. 2020). Endocrine disruptors can be effective at low concentrations and can perturb critical molecular events when introduced at critical windows during embryonic development (Heindel 2019; Jirtle and Skinner 2007; Rissman and Adli 2014; Schug et al. 2011). The pollutant, 2,3,7,8-tetrachlorodibenzo-*p*-dioxin (TCDD), is generated as a by-product of diverse industrial processes, as well as during waste incineration, resulting in its wide environmental dissemination and actions as an endocrine disruptor (Poland and Knutson 1982). TCDD induces the aryl hydrocarbon receptor (AHR) signaling pathway (Denison and Nagy 2003; Schmidt and Bradfield 1996). AHR is a member of the basic helix–loop–helix (bHLH) family of transcription factors and is unique in its activation by ligands (Avilla et al. 2020; McIntosh et al. 2010). In the absence of a ligand, AHR is present in the cytoplasm in a latent state bound to chaperone proteins and other regulatory proteins (Avilla et al. 2020; Dietrich and Kaina 2010; Gu et al. 2000; Petrulis and Perdew 2002; Wright et al. 2017). Upon ligand

Address correspondence to Khursheed Iqbal, The University of Kansas Medical Center, 3901 Rainbow Boulevard, Kansas City, KS 66160 USA. Email: kiqbal@kumc.edu or Michael J. Soares, The University of Kansas Medical Center, 3901 Rainbow Boulevard, Kansas City, KS 66160 USA. Email: msoares@kumc.edu

Supplemental Material is available online (https://doi.org/10.1289/EHP9256).

*Current address: Stephen H. Pierce, Genome Medicine Center, Children's Mercy, Kansas City, Missouri, USA.

†Current address: Pramod Dhakal, Department of Animal Sciences, University of Missouri, Columbia, Missouri, USA.

The authors declare they have no actual or potential competing financial interests.

Received 3 March 2021; Revised 6 October 2021; Accepted 18 October 2021; Published 8 November 2021.

binding, AHR translocates into the nucleus and heterodimerizes with the AHR nuclear translocator (ARNT) via shared per–Arnt–Sim domains and regulates gene transcription (Beischlag et al. 2008; Gu et al. 2000). This classical/canonical pathway for AHR action has been extensively investigated and implicated in drug metabolism and in a wide variety of physiological and pathological processes (McMillan and Bradfield 2007; Mulero-Navarro and Fernandez-Salguero 2016; Ramadoss et al. 2005). AHR can also act in a nonclassical/noncanonical mode to influence an assortment of signaling pathways that affect cell function (Avilla et al. 2020; Dietrich and Kaina 2010; Wright et al. 2017).

Exposure to TCDD can affect pregnancy success and aspects of placental and fetal growth (Birnbaum 1994; Burns et al. 2013; Gray et al. 1997; Hurst et al. 2000; Ishimura et al. 2009), and genomic imprinting (Iqbal et al. 2015; Kang et al. 2011) in the rodent placenta. These actions are dependent upon dose and timing of exposure. Some evidence for adverse pregnancy outcomes following TCDD exposure has been reported in the human (Wesselink et al. 2014). In this study, we investigated the effects of TCDD exposure on placental development in the rat.

Methods

Chemicals

TCDD (99.8% purity; D-404S), Aroclor 1254 (99.8% purity; APP-9-163-10X), polychlorobiphenyl 126 (PCB126; 99.8% purity; C-126N), and benzo[*a*]pyrene (BaP; 99.8% purity; H169N) were obtained from AccuStandard, solubilized in dimethyl sulfoxide (DMSO; D8418; Sigma-Aldrich), and delivered in corn oil (405435000; Acros Organics/ThermoFisher). The control corn oil preparation delivered to rats included the same amount of DMSO used to initially solubilize the AHR ligands.

Animals

Holtzman Sprague-Dawley rats were obtained from Envigo and maintained under specific pathogen-free conditions in an Association for Assessment and Accreditation of Lab Animal Care–accredited facility at the University of Kansas Medical Center (KUMC; Kansas City, KS). Rats were maintained in a 14-h light:10-h dark photoperiod and fed standard rat chow and water *ad libitum*. Timed pregnancies were established by mating adult female rats (8–10 wk of age) with adult male rats (>10 wk of age). Presence of sperm or a seminal plug in the vagina was designated gestation day (GD) 0.5. Pseudopregnant females were generated by mating adult female rats (8–10 wk of age) with adult vasectomized male rats (>10 wk of age). Detection of seminal plugs was designated Day 0.5 of pseudopregnancy. TCDD [2–20 μg/kg body weight (BW)] or the corn oil vehicle control was administered once by oral gavage in a volume of 2.5 mL/kg. The DMSO concentration in the treatments was 0.2%. Adult male rats (10 wk of age) were treated and euthanized 5 d later by carbon dioxide (CO_2) asphyxiation and thoracotomy, whereas pregnant females were treated on GD6.5 and similarly euthanized at GD13.5 or 18.5. The health of each pregnancy was determined, and tissues were collected for biochemical and histological analysis. Failed placental–fetal units were identified by the presence of hemorrhage, necrosis, and anemic and growth restricted fetuses. Fetal survival rate was calculated on a per pregnancy basis as the number of live fetuses/total fetuses times 100. Tissues used for biochemical analysis (adult liver, lung, and spleen; placentation site; and fetal liver and brain) were snap frozen in liquid nitrogen and stored at −80°C until processed, whereas tissues for histological analysis (placentation sites and whole fetuses) were frozen in dry ice–cooled heptane and stored at −80°C until processed. Analyses were performed on tissues randomly selected from each pregnancy. A total of 386 pregnant females (326: treated; 60: untreated) and 130 male rats were used in this study. Pregnancies in the Holtzman Sprague-Dawley rat were obtained at an efficiency of 96% of all mated females. All animal protocols were approved by the KUMC Institutional Animal Care and Use Committee (approval no. 2019–2495).

Generation of Ahr and Cyp1a1 Mutant Rats

Targeted mutations were generated using clustered regularly interspaced palindromic repeats (CRISPR)/CRISPR associated protein 9 (Cas9) genome editing (Iqbal et al. 2021). For *Ahr* gene editing, a single guide RNA (gRNA) was designed, synthesized, and validated by the Genome Engineering Center at Washington University (St. Louis, MO). The gRNA was targeted to Exon 2 of the *Ahr* gene, which encodes the bHLH DNA binding domain (target sequence: CTTCTAAACGACACAGAGACCGG; corresponding to NM_001308254). The cytochrome P450 1A1 gene (*Cyp1a1*) was targeted using duplex *CRISPR* RNA (crRNA) (Alt-R CRISPR-Cas9 crRNA; 425286668; Integrated DNA Technologies) and trans-activating *CRISPR* RNA (tracrRNA) (1072532; Integrated DNA Technologies). Functional *Cyp1a1* gRNAs were generated by incubating crRNAs and tracrRNAs at 95°C for 5 min and then cooled slowly at room temperature before use. gRNAs targeting Exon 1 (TCCAAGGCAGAATGTGGTGACGG) and Exon 7 (GGGGTGATCCAAACGAGTTCCGG; corresponding to NM_012540.2) of the *Cyp1a1* gene were used to generate mutations.

Genome editing reagents were microinjected or electroporated into rat embryos on the basis of previously described procedures (Iqbal et al. 2009; Kaneko 2017a, 2017b; Shao et al. 2014). In brief, 4- to 5-wk-old donor female rats were intraperitoneally injected with 30 U of equine chorionic gonadotropin (eCG; G4877; Sigma-Aldrich), followed by an intraperitoneal injection of 30 U of human chorionic gonadotropin (hCG; C1063; Sigma-Aldrich) 48 h later and then immediately mated with adult male rats. Zygotes were flushed from oviducts with M2 medium at GD0.5 and maintained in M2 medium (MR-015-D; EMD Millipore) supplemented with bovine serum albumin (A9647; Sigma-Aldrich) at 37°C in 5% CO_2 for 2 h. Zygotes were microinjected with a mixture of *Ahr* gRNA (25 ng/μL) and Cas9 mRNA (30 ng/μL; Genome Engineering Center, Washington University) prepared in Tris-ethylenediaminetetraacetic acid (TE) buffer (pH 7.4). Microinjections were performed using a Leica inverted microscope (Leica Biosystems) and an Eppendorf microinjection system. For *Cyp1a1*, zygotes were electroporated with a mixture of gRNAs for *Cyp1a1* (35 ng/μL) and Cas9 protein (1081058; Integrated DNA Technologies) with a nuclear localization signal (1 ng/μL) prepared in TE buffer (pH 7.4). The NEPA21 electroporator (Nepa Gene Co. Ltd.) was used to transfer the gene editing reagents. Parameters for the poring pulse were 225 V, 1-ms pulse width, 50-ms pulse interval, 4 pulses, 10% decay rate, with positive polarity, whereas parameters for the transfer pulse were 20 V, 50-ms pulse width, 50-ms pulse interval, 5 pulses, 40% decay rate, with positive or negative polarity. Manipulated zygotes were transferred to oviducts of Day-0.5 pseudopregnant rats (20–30 zygotes per rat and at least 6 embryo transfers performed for *Ahr* and *Cyp1a1*).

Offspring were screened for mutations at specific target sites within each edited gene. For initial screening, genomic DNA was purified from tail-tip biopsies using the Extract-N-Amp Tissue Polymerase Chain Reaction (PCR) Kit (Sigma-Aldrich). Potential mutations within target loci were screened by designing specific PCR primers to determine the boundaries of the deletions by DNA sequencing (Genewiz Inc.). PCR primers used for genotyping of the genetically altered rats are listed in Table S1. Germline

transmission of the mutated genes was determined in the F_1 offspring by backcrossing founder (F_0) rats with wild-type (WT) rats. Detection of mutations in F_1 offspring identical to the mutation from F_0 parents was considered confirmation of germline transmission. *Ahr* and *Cyp1a1* mutant rat models are available at the Rat Resource & Research Center (RRRC nos. 831 and 890; University of Missouri, Columbia, MO; https://www.rrrc.us).

Functional Validation of Ahr and CYP1A1 Mutant Rats

Ten-wk-old male AHR mutant rats and WT littermates were administered either a single oral dose of TCDD (25 μg/kg BW), Aroclor 1254 (50 mg/kg BW), PCB126 (100 μg/kg BW), BaP (100 mg/kg BW), or the corn oil vehicle ($n = 5$/group). Ten-wk-old male CYP1A1 mutant rats and WT littermates were administered either a single oral dose of TCDD (25 μg/kg BW) or the corn oil vehicle ($n = 3$–5/group). Rats were euthanized 5 d postexposure. Liver and thymus tissues from control and TCDD treatments were collected and weighed. Hepatic tissue from all treatments was frozen for subsequent biochemical analyses.

CYP1A1 Enzyme Activity Assay

CYP1A1 activity was measured using the P450-Glo CYP1A1 assay kit (V8751; Promega), according to the manufacturer's instructions. Liver tissue ($n = 3$–5 per group WT or AHR Null exposed to either oil control or 25 μg/kg BW TCDD) was minced and homogenized in 100 mM of potassium phosphate buffer (pH 7.4) using a Potter-Elvehjem homogenizer (ThermoFisher). Supernatants were collected by centrifugation at $9{,}000 \times g$ for 10 min and then centrifuged at $60{,}000 \times g$ for 1 h in an Optima TL ultracentrifuge (Beckman Coulter) to obtain microsomes (Knights et al. 2016). Liver microsomes (20 μg) were mixed with luciferin-chloroethyl ether (substrate) for 10 min at room temperature. After preincubation, a reduced nicotinamide adenine dinucleotide phosphate (NADP) (NADPH)-regenerating system solution (2.6 mM $NADP^+$, 6.6 mM glucose-6-phoshate, 0.4 U/mL glucose-6-phoshate dehydrogenase, and 6.6 mM magnesium chloride) was added and the mixture incubated at 37°C for 30 min. Generation of luciferin was detected by adding the luciferin detection reagent included in the P450-Glo CYP1A1 assay kit, and luminescence was determined using a luminometer (model TD-20/20; Turner BioSystems) and reported as relative fluorescence units.

Ovulatory Responses to Exogenous Gonadotropins

Four- to 5-wk-old female rats ($n = 6$ per group, WT or AHR null) were examined for responsiveness to exogenous gonadotropins. Females were injected intraperitoneally with eCG (30 IU) at 1700 hours, followed by an injection of hCG (30 IU) 48 h later. Twenty-four hours after the hCG administration, animals were euthanized, oocytes were flushed from the oviduct with M2 medium, cumulus cells were denuded using hyaluronidase (10 mg/mL for 5 min, H3631, Sigma-Aldrich), and oocytes were counted.

Fertility Tests

Fertility tests were performed by mating 12- to 16-wk-old male rats with 8- to 12-wk-old female rats for 12 wk and assessing pregnancies and litter sizes ($n = 6$ per genotype pairing). Mutant or WT males were paired with WT females, and mutant or WT females were paired with fertile WT males. Vaginal lavage was performed daily to verify estrous cyclicity, mating (presence of sperm), and signs of pregnancy (continuous diestrus). Litter sizes of pregnancies were also monitored.

In Vitro Analysis of Trophoblast and Arterial Endothelial Cell Responses to TCDD

Blastocyst-derived rat trophoblast stem (TS) cells previously generated in our laboratory (Asanoma et al. 2011) were cultured in rat TS cell medium [RPMI 1640, 20% (vol/vol) fetal bovine serum (FBS; ThermoFisher), 100 μm 2-mercaptoethanol (M7522; Sigma-Aldrich), 1 mM sodium pyruvate (11360-070; ThermoFisher), 50 μM penicillin (15140122; ThermoFisher), and 50 U/mL streptomycin (15140122; ThermoFisher)] supplemented with 70% rat embryonic fibroblast conditioned medium prepared as previously described (Asanoma et al. 2011), fibroblast growth factor 4 (37.5 ng/mL; 100-31; Peprotech), and heparin (1.5 μg/mL; H3149; Sigma-Aldrich). Rat arterial endothelial cells were purchased from VEC Technologies, Inc. and maintained in MCDB-131 complete culture medium. Cells were plated in 962-mm^2 wells at ~50–60% confluence and treated 12 h after plating. Cells were exposed to vehicle control (i.e., DMSO) or TCDD at 10 or 100 μM, concentrations known to induce CYP1A1 *in vitro* (Knutson and Poland 1980). The DMSO concentration in the cell cultures was 0.05%. After 24 h, cells were harvested, medium removed, and total RNA isolated.

Transcript Analysis

Total RNA was extracted from cells ($n = 6$) and tissues ($n = 5$–6) using TRI Reagent Solution (AM9738; ThermoFisher). Complementary DNAs (cDNAs) were synthesized from total RNA (1 μg) for each sample using SuperScript 2 reverse transcriptase (18064014; ThermoFisher), diluted 5 times with water, and subjected to quantitative PCR (qPCR) to estimate mRNA levels. Real-time qPCR (RT-qPCR) primers were designed using Primer3 (https://bioinfo-ut.ee/primer3), obtained from Integrated DNA Technologies, and sequences are presented in Table S2. RT-PCR of cDNAs was carried out in a reaction mixture (10 μL) containing SYBR Green PCR Master Mix (4309155; Applied Biosystems) and primers (200 nM each). Amplification and fluorescence detection were carried out using the ABI 7500 RT-PCR system (Applied Biosystems). PCR was performed under the following conditions: 95°C for 5 min, followed by 35 cycles at 95°C for 30 s, 60°C for 30 s, and 72°C for 30 s. The delta-delta Ct method was used for relative quantification of gene expression for each sample normalized to 18S RNA, which was stable among the conditions and tissues tested, as shown in Table S3.

Flow Cytometry

Uterine mesometrial compartments associated with placentation sites (termed the metrial gland) were dissected from GD13.5 pregnant females ($n = 3$), as previously reported (Ain et al. 2006). Harvested metrial glands were minced and then incubated in collagenase I (17100017; ThermoFisher) for 30 min to dissociate the tissue and liberate natural killer (NK) cells. Dissociated cells were passed through a 70-μm cell strainer (10199-656; VWR) and incubated with ammonium–chloride–potassium (ACK) buffer (A1049201; ThermoFisher) to lyse erythrocytes. Cells (1×10^6) were incubated for 30 min with 2% FBS (Sigma-Aldrich) and 5 μg/mL rat immunoglobulin G (IgG; 550617; ThermoFisher) to block nonspecific antibody binding sites, then incubated for 40 min with phycoerythrin-conjugated mouse antirat CD161 (550270; BD Pharmingen). All cells were washed in phosphate buffered saline (PBS; pH 7.4) containing 2% FBS. Cells were then analyzed using a BD LSRII flow cytometer (BD Biosciences).

Western Blotting

Tissues were collected in radioimmunoprecipitation assay lysis buffer (sc-24948A; Santa Cruz Biotechnology) with a protease inhibitor cocktail (11697498001; Sigma-Aldrich), homogenized for 30 s using a PRO300A tissue homogenizer (Pro Scientific), and centrifuged at $5{,}000 \times g$ for 5 min. Protein concentrations of supernatants were determined using the DC Protein Assay Kit (5000112; Bio-Rad Laboratories). Protein preparations (10 μg/lane) were separated on sodium dodecyl sulfate–polyacrylamide gels and transferred to Immun-blot polyvinylidene difluoride (PVDF) membranes (10600023; GE Healthcare) for 1 h at 4°C. The PVDF membranes were blocked in 5% nonfat milk in PBS-Tween 20 (0.1%) for 1 h at room temperature. Antibodies against AHR (1:500 dilution; BML-SA210; Enzo Life Sciences, Inc.), CYP1A1 (1:2,000 dilution; A3001; XenoTech), and glyceraldehyde-3-phosphate dehydrogenase (GAPDH; 1:10,000 dilution; AB2302; Millipore) were diluted in 5% nonfat milk in PBS-Tween 20 and incubated at 4°C overnight. Immunoreactive proteins were detected with secondary antibodies consisting of horseradish peroxidase (HRP)–conjugated goat antirabbit IgG (1:8,000 dilution; 7074P2; Cell Signaling) and HRP-conjugated rabbit antimouse IgG (1:10,000 dilution; A9044rat; Sigma-Aldrich) and the Luminata Crescendo Western HRP substrate (WBLUR0100; EMD Millipore). Chemiluminescence was detected by exposure to Radiomat LS autoradiography film (Agfa HealthCare) followed by processing in a tabletop X-ray radiograph film processor (Konica Minolta SRX-101A).

Immunohistochemistry

Immunohistochemical analyses were performed on 10-μm frozen tissue sections ($n = 3$ per group, oil- or TCDD-treated WT rats). Cryosections were prepared with a Leica CM 1850 cryostat (Leica Biosystems). Primary antibodies to rat CYP1A1 (1:500 dilution; A3001; XenoTech), RECA-1 antibody (1:100 dilution; MCA970GA; Bio-Rad), pan-cytokeratin (1:1,000 dilution; F3418; Sigma-Aldrich), perforin (1:1,000 dilution; TP251; Torrey Pines Biolabs), and CD31 (1:500; 550274; BD Pharmingen) were used. Indirect immunofluorescence detection used goat antimouse IgG tagged with Alexa 488 (1:1,000 dilution; A11029; ThermoFisher) or goat antirabbit IgG tagged with Alexa 568 (1:400 dilution; A11031; ThermoFisher). Tissue sections were incubated with primary antibodies at 4°C for 12 h and with secondary antibodies at room temperature for 2 h. Negative controls were performed with normal rabbit serum or isotype-specific control mouse IgG and did not exhibit positive reactivity in tissue sections. Flourmount-G with 4′6-diamidino-2-phenylindole (00-4959-52; ThermoFisher) was used as a medium for slide mounting and for visualizing nuclei. Four to six tissue sections were processed for each antibody per treatment group. Processed tissue sections were inspected, and images captured with a Nikon Eclipse 80i upright microscope equipped with a charge-coupled device camera (Nikon). Measurements of the depth of invasion were performed with National Institutes of Health Image J software (Konno et al. 2007; Rosario et al. 2008). Depth of invasion was calculated as the ratio of the distance of trophoblast cell (cytokeratin positive) migration from the junctional zone into the uterus vs. the total distance between the junctional zone and the outer surface of the uterus. Assessment of the depth of invasion was performed at the center of each placentation site.

RNA-Sequencing

Transcript profiles were determined by RNA-Sequencing (RNA-seq) of GD13.5 metrial gland (uterine–placental interface) from oil- and TCDD-treated rats. Total RNA was extracted from the tissue using TRIzol Reagent (ThermoFisher), according to the manufacturer's instructions. RNA quantification was performed using a Nanodrop spectrophotometer (ThermoFisher) and 500 ng of total RNA was used for RNA-seq library preparation. Libraries were prepared from RNA by using a TruSeq standard mRNA kit (RS-122-2101; Illumina), according to the manufacturer's instructions. Briefly, mRNA was enriched from total RNA by oligo-dT magnetic beads and purified, and then mRNA was chemically fragmented. The first strand of cDNA was synthesized by using random hexamer primers and reverse transcriptase. AMPure XP beads (A63880; Beckman Coulter) were used to separate double-stranded cDNA from the second strand reaction mix. cDNA ends were blunted and polyadenylic acid tails added to the 3′ ends. Finally, after ligation of indexing adaptors (Illumina), the suitable DNA fragments were selected for PCR amplification for 15 cycles. cDNA libraries were prepared for the oil- and TCDD-treated groups ($n = 4$ for each) and sequenced at the KUMC Genomics Core.

RNA-seq data were analyzed using CLC Genomics Workbench (Qiagen). High-quality reads were aligned to the *Rattus norvegicus* reference genome (Rnor_6.0). Only reads with <2 mismatches and minimum length and a similarity fraction of 0.8 were mapped to the reference genome. Gene expression values were reported as reads per kilobase of transcript per million mapped reads. Transcripts that exhibited more than 1.5-fold change ($p < 0.05$, Benjamini and Hochberg correction for false discovery rate) were considered differentially expressed genes. Ingenuity Pathway Analysis (Qiagen) was used to identify the predominant signaling pathways and molecules affected by the treatments. RT-qPCR was used to validate the RNA-seq results. The RNA-seq data set is available at the Gene Expression Omnibus (GEO) website (https://www.ncbi.nlm.nih.gov/geo/; accession no. GSE166604).

Metrial Gland Cell Isolation for Single Cell RNA-Seq

Metrial glands were collected from GD13.5 rat placentation sites (Ain et al. 2006) and transferred to ice cold Hank's Balanced Salt Solution (HBSS) ($n = 2$ per group). Tissues were minced into fine pieces with a razor blade and digested with an enzymatic cocktail consisting of Dispase II (1.25 U/mL; D4693; Sigma-Aldrich) and collagenase IV (0.4 mg/mL; C5138; Sigma-Aldrich) in HBSS at 37°C for 30 min. Cell suspensions were incubated with ACK buffer (ThermoFisher) at room temperature for 5 min to lyse red blood cells. Cells were washed with HBSS containing 2% FBS (vol/vol) and DNase1 (80 U/mL), and filtered through a 100-μm cell strainer. Debris was removed using MACS Debris Removal Solution (130-109-398, Miltenyi Biotec), and the cells were filtered through a 40-μm cell strainer. Cell numbers were counted and viabilities determined by propidium iodide exclusion staining followed by flow cytometry. Cell viabilities were between 90% and 93%.

Peripheral Blood Mononuclear Cell Isolation for Single Cell RNA-Seq

Peripheral blood mononuclear cells (PBMCs) were isolated using Histopaque (1083-1, Sigma-Aldrich). Briefly, heparinized blood was collected from rats by cardiac puncture and layered on Histopaque and centrifuged at $400 \times g$ for 30 min ($n = 2$ per group). The supernatant was removed and the cell layer incubated with ACK buffer (ThermoFisher) at room temperature for 5 min to lyse red blood cells. PBMCs were collected by centrifugation at $400 \times g$ for 5 min, washed with PBS, and collected by centrifugation at $400 \times g$ for 5 min. Cells were resuspended in HBSS, numbers counted, and viabilities determined by propidium iodide exclusion staining followed by flow cytometry. Cell viabilities were >95%.

Single Cell RNA-Seq

Single cells were captured by the Chromium Controller into 10× barcoded gel beads and library preparation was performed using Chromium Single Cell 3′ (version 3 chemistry; 10x Genomics). Libraries were sequenced using a NovaSeq 6000 sequencer (Ilumina). Library preparation and sequencing were performed by the KUMC Genomics Core.

Single Cell RNA-Seq Data Analysis

The Cell Ranger pipeline was used to process and analyze the single cell sequencing data. *Cellranger mkfastq/bcl2fastq* was used to convert raw base call files to FASTQ files followed by demultiplexing libraries based on sample indices. *Cellranger count* was used to perform alignment, filtering, barcode counting, and unique molecular identifier counting and to generate read count matrices from the FASTQ files. Reads were aligned to Rnor_6.0 reference genome using the Spliced Transcripts Alignment to a Reference aligner. A rat reference genome was custom built using masked Rnor_6.0 genome assembly and gene annotations [in General Feature Format (GTF)] downloaded from ENSEMBL using the *cellranger mkref* command. The *Cellranger mkgtf* utility was used to filter pseudogenes in GTF files. For sample aggregation, *Cellranger count* outputs were integrated and normalized using the *Cellranger aggr* command. Further reanalysis was done using the *Cellranger reanalyze* pipeline.

Additional data analysis was performed within the Seurat pipeline (version 3.1.5) (Stuart et al. 2019). To cluster cells, we imported genes by cell matrices to Seurat, merged replicates, and created Seurat objects, which was followed by filtering doublets, empty droplets, and cells with high mitochondrial sequences with the following parameters (subset = nFeature_RNA > 200 & nFeature_RNA < 3000 & percent.mt < 20). We filtered the data set and accepted genes that were expressed by a minimum of three cells. Oil- and TCDD-treated data was integrated using *FindIntegrationAnchors/IntegrateData* (dims = 1:20). Integrated raw counts were normalized and log transformed, and variable genes were identified with the *FindVariableFeatures* function (using default parameters). The JackStrawPlot function in Seurat was used to find significant principle components (PCs) for each data set and used to create uniform manifold approximation and projection (UMAP) plots. PCs were used to create a *k*-nearest neighbors graph with the *FindNeighbors* function (dims = 1:20) and clustered cells with the *FindClusters* function (resolution = 0.05). Cluster-specific gene expression was determined using *FindConservedMarkers*. For cluster visualization and individual gene visualization on all clusters, we used the *RunUMAP* function (dims = 1:20). Specific cell types in the metrial gland (stromal: *Mmp2*, *Timp2*; mesenchymal: *Col1a1*, *Col3a1*; NK cells: *Prf1, Nkg7*; macrophages: *Cd74, Csf1r*; endothelial cells: *Cdh5, Adgrl4*; smooth muscle cells: *Acta2, Tagln*), and PBMCs (T cells: *Cd3e, Cd3g*; monocytes: *Csf1r, Cd68*; B cells: *Cd79, Cd83*; NK cells: *Gzma, Nkg7*) were identified on the basis of known expression profiles.

To perform differential gene expression analysis within clusters across treatments, we used the *FindMarkers* function from the Seurat 3 package (logfc.threshold = 0.15) (Stuart et al. 2019), which uses the nonparametric Wilcoxon rank sum test for single-cell gene expression. The level of statistical significance for treatment-specific transcriptomic changes was set at a $p < 0.05$ and a $\log_2$-fold change ≥ 0.15 or ≤ -0.15. The single cell RNA-Seq (scRNA-seq) data set is available at the GEO website (https://www.ncbi.nlm.nih.gov/geo/: metrial gland accession no. GSE166659, PBMCs accession no. GSE178407).

The Database for Annotation Visualization and Integrated Discovery Bioinformatics Resources 6.8 (https://david.ncifcrf.gov/) tool was used to perform functional enrichment and pathway analyses. The CellPhoneDB tool was used to identify ligand–receptor interactions from the scRNA-seq analysis (Efremova and Vento-Tormo 2021).

Statistical Analysis

Values are expressed as the mean ± standard error of the mean (SEM). Statistical comparisons between two means were performed with the nonparametric Wilcoxon rank sum test. Comparisons between more than two groups were made using analysis of variance and post hoc comparisons of multiple means performed using the Tukey's post hoc test.

Results

Maternal and Fetal Responses to TCDD

Initially, we evaluated the effects of various doses of TCDD on pregnancy in the rat (Figure 1A). Pregnant rats were administered a single gavage of vehicle or 2, 8, 12, or 20 μg/kg BW of TCDD on GD6.5, and the viability of litters was assessed at GD13.5. This represents an interval after embryo implantation critical for placental morphogenesis. Administration and dosage of TCDD were comparable to previous experimentation examining the effects of TCDD on rat pregnancy and placentation (Ishimura et al. 2002, 2006; Kransler et al. 2007; Wu et al. 2014). Rats exposed to TCDD had less viable conceptuses, and this difference appeared to be dose dependent. Rats treated with TCDD concentrations of 8 μg/kg BW and higher had significantly higher percentages of pregnancy loss than those of the control group (Figure 1B). Maximal pregnancy loss was observed at a TCDD concentration of 20 μg/kg BW. We used *Cyp1a1* transcript expression as a measure of AHR activation and TCDD activity. Each of the tested concentrations of TCDD maximally activated AHR signaling, as assessed by measuring hepatic *Cyp1a1* transcript levels (Figure 1C); similarly, rats treated with 2 μg/kg BW had significantly higher spleen and lung *Cyp1a1* transcript levels (Figure 1D). At 2 μg/kg BW, neither fetal nor placental weights or fetal/placental weight ratios differed between oil- and TCDD-treated rats assessed at GD18.5 (Figure 1E); however, this maternally administered TCDD concentration resulted in higher levels of *Cyp1a1* transcripts in fetal liver and brain, which we used as a proxy for AHR activation (Figure 1G). This was supported by higher levels of CYP1A1 protein in the fetal liver, as determined by immunohistochemistry (Figure 1F). We selected TCDD doses of 2 and 20 μg/kg BW for subsequent analyses. We chose a dose of 2 μg/kg BW of TCDD because fetuses gestationally exposed to this dose demonstrated higher CYP1A1 protein expression, suggesting activation of AHR signaling, without a significant difference in viability from controls. In contrast, the 20-μg/kg BW TCDD dose was selected because it resulted in fetal demise and extensive pregnancy loss.

Analysis of the Effects of TCDD on Placentation

Placentation sites were examined from pregnant females treated with TCDD (2 μg/kg BW or oil). Treatments were administered on GD6.5 (embryo implantation occurs on GD5.5) and placentation sites examined on GD13.5 (Figure 2A). A similar structural organization of placentas into junctional and labyrinth zone compartments was observed in both oil- and TCDD-treated pregnancies. However, a striking difference was seen in the presence of cytokeratin-positive invasive trophoblast cells within the metrial gland of TCDD- but not oil-treated pregnant rats (Figure 2B). These invasive trophoblast cells were specifically targeted to uterine spiral arteries, where they effectively supplanted the vascular endothelium. Significantly deeper intrauterine endovascular trophoblast cell invasion was

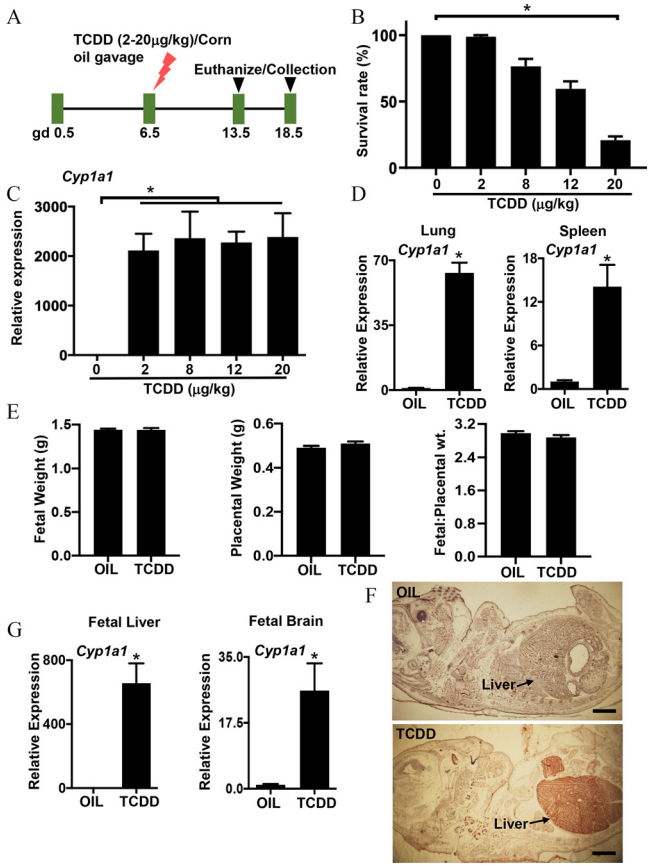

Figure 1. Effect of TCDD exposure on pregnancy outcomes. (A) Schematic showing the treatment plan used in this study. Rats were treated on GD6.5 with corn oil (OIL) or TCDD and euthanized on GD13.5 or 18.5. (B) Fetal survival rate (%) after TCDD treatment as assessed on GD13.5 ($n=5$ pregnancies/group), *, $p<0.0001$. Fetal survival rate was calculated on a per pregnancy basis as the number of live fetuses/total fetuses times 100. (C) Detection of *Cyp1a1* transcript levels in liver tissues of GD13.5 pregnant females exposed to OIL or different concentrations of TCDD using RT-qPCR ($n=5$ pregnancies/group), *, $p=0.006$. (D) *Cyp1a1* expression in lung and spleen of OIL- or TCDD (2 μg/kg BW)-exposed pregnant rats at GD13.5 measured by RT-qPCR ($n=5$ pregnancies/group; lung, *, $p=0.0079$; spleen, $p=0.0079$). (E) Fetal and placental weights and fetal/placental weight ratio at GD18.5 following OIL or TCDD treatment (2 μg/kg BW) ($n=5$ pregnancies/group). (F) Representative images for CYP1A1 immunohistochemistry of embryonic day (ED) 18.5 fetus from pregnant rats treated with OIL or TCDD (2 μg/kg BW). Scale bar: 1 mm. (G) RT-qPCR measurement of *Cyp1a1* transcripts in ED18.5 brain and liver tissues from OIL- or TCDD (2 μg/kg BW)-treated pregnant rats ($n=5$ pregnancies/group; fetal liver, *, $p=0.0079$; fetal brain, *, $p=0.0079$). Transcript expression level is relative to control. The delta-delta Ct method was used for relative quantification of gene expression for each sample normalized to 18S RNA. Data presented in (B) and (C) were analyzed using a one-way ANOVA followed by Tukey's multiple comparison post hoc test and the Wilcoxon rank sum test (D, E, and G). The asterisks denote a statistically significant difference from the corresponding control. Bar graphs represent the mean ± SEM. The mean and SEM values for data presented in this figure are shown in Tables S4–S8. Note: ANOVA, analysis of variance; BW, body weight; Cyp1a1, cytochrome P450, family 1, subfamily a, polypeptide 1; GD, gestation day; RT-qPCR, real-time quantitative polymerase chain reaction; SEM, standard error of the mean; TCCD, 2,3,7,8-tetrachlorodibenzo-*p*-dioxin.

observed in TCDD-exposed placentation sites (Figure 2C,D). Furthermore, analysis of invasive trophoblast cell-specific transcripts, *Prl5a1* and *Prl7b1* (Ain et al. 2003; Rosario et al. 2008; Wiemers et al. 2003), revealed significantly higher expression in the metrial gland of TCDD-exposed pregnancies (Figure 2E).

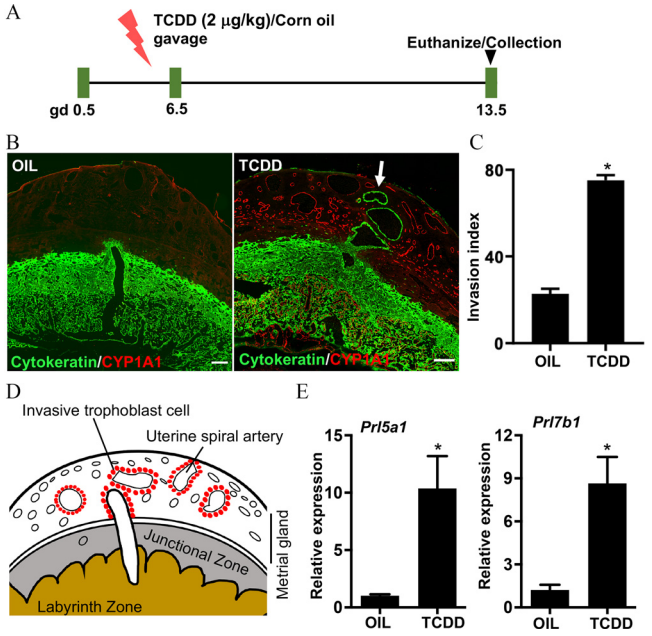

Figure 2. Measures of intrauterine endovascular trophoblast cell invasion in rats with gestational TCDD exposure. (A) Schematic showing the treatment plan used in this study. Rats were treated on GD6.5 with corn oil (OIL) or TCDD (2 μg/kg BW) and euthanized on GD13.5. (B) Representative images for pan-cytokeratin (green) and CYP1A1 (red) immunostaining of GD13.5 placentation sites. The white arrow shows the depth of intrauterine endovascular trophoblast cell invasion. Scale bar: 500 μm. (C) Quantification of the depth of cytokeratin-positive cell penetration into the uterine mesometrial vasculature ($n=4$–6/group, *, $p=0.0001$). Depth of invasion was calculated as the ratio of the distance of trophoblast cell (cytokeratin positive) migration from the junctional zone into the uterus vs. the total distance between the junctional zone and the outer surface of the uterus. Assessments of the depth of invasion were performed at the center of each placentation site. (D) Schematic diagram depicting the metrial gland (uterine–placental interface). (E) RT-qPCR measurements of *Prl5a1* and *Prl7b1* transcripts in GD13.5 metrial gland tissues isolated from OIL- and TCDD-treated rats ($n=5$/group; *Prl5a1*, *, $p=0.0022$; *Prl7b1*, *, $p=0.0022$). Transcript expression level is relative to control. The delta-delta Ct method was used for relative quantification of gene expression for each sample normalized to 18S RNA. The level of significance was determined using the Wilcoxon rank sum test. Asterisks denote statistically significant differences from the corresponding controls. Bar graphs represent the mean ± SEM. The mean and SEM values for data presented in this figure are shown in Tables S9 and S10. Note: BW, body weight; Cyp1a1, cytochrome P450, family 1, subfamily a, polypeptide 1; GD, gestation day; Prl5a1, prolactin family 5, subfamily a, member 1; Prl7b1, prolactin family 7, subfamily b, member 1; RT-qPCR, real-time quantitative polymerase chain reaction; SEM, standard error of the mean; TCCD, 2,3,7,8-tetrachlorodibenzo-*p*-dioxin.

Evaluation of TCDD and Other Environmentally Relevant AHR Ligand Effects in AHR Null Rats

To investigate the role of AHR signaling in mediating TCDD actions on placental development, we used WT and AHR null pregnant rats. We first generated an AHR null rat model using CRISPR/Cas9 gene editing (Figure 3A; Figure S1). AHR heterozygote male × AHR heterozygote female breeding generated offspring with the expected Mendelian pattern of inheritance (Figure 3B). Homozygous disruption of the bHLH domain of AHR eliminated the presence of immunoreactive AHR protein (Figure 3C) and resulted in a failure of TCDD stimulated hepatic *Cyp1a1*, cytochrome P450, family 1, subfamily b, polypeptide 1 (*Cyp1b1*), and aryl-hydrocarbon receptor repressor *(Ahrr)* transcript levels (Figure 3D) and TCDD-induced hepatic growth and thymic regression (Figure S2A,B). Additional AHR activators, including Aroclor 1254 (a mixture of AHR ligands), PCB126,

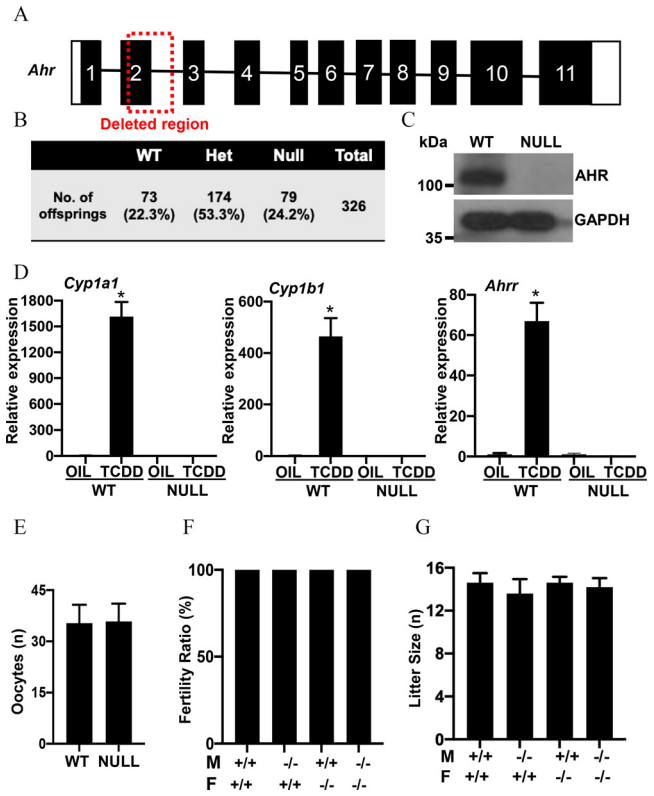

Figure 3. Generation of an AHR null rat model. (A) Schematic representation of the strategy for targeting Exon 2 of the Ahr gene. A red dashed line depicts the 342-bp deleted region. (B) Mendelian ratios of AHR heterozygous breeding and viability of AHR nulls. (C) Representative image of western blot analysis of AHR protein expression in WT and AHR null liver tissues. GAPDH was used as an internal control. (D) Transcript analysis of AHR target genes (*Cyp1a1*, *Cyp1b1*, and *Ahrr*) in WT and null (NULL) rat liver following corn oil (OIL) or TCDD (25 μg/kg BW) treatment ($n = 5$/group): *Cyp1a1*, *Cyp1b1*, and *Ahrr*, $p < 0.0001$. The delta-delta Ct method was used for relative quantification of gene expression for each sample normalized to 18S RNA. (E) Number of ovulated oocytes recovered per female after gonadotropin stimulation of 4- to 5-wk-old WT or AHR null female rats ($n = 6$/group). (F) Pregnancy success rates (sperm-positive females that became pregnant) of WT (+/+) and AHR null (–/–) rats in various breeding combinations ($n = 6$/combination). (G) Average litter sizes from pregnancies generated by WT (+/+) and AHR null (–/–) rats in various breeding combinations ($n = 6$/combination). Transcript expression level is relative to oil-treated respective genotype. The level of significance was determined using either the Wilcoxon rank sum test or a one-way ANOVA followed by Tukey's multiple comparison post hoc test where appropriate. Asterisks denote a statistically significant difference from the corresponding control. Bar graphs represent the mean ± SEM. The mean and SEM values for data presented in this figure are shown in Tables S11–S14. Note: AHR, aryl hydrocarbon receptor; Ahrr, aryl-hydrocarbon receptor repressor; ANOVA, analysis of variance; BW, body weight; Cyp1a1, cytochrome P450, family 1, subfamily a, polypeptide 1; Cyp1b1, cytochrome P450, family 1, subfamily b, polypeptide 1; F, female; GAPDH, glyceraldehyde 3-phosphate dehydrogenase; Het, heterozygous; M, male; SEM, standard error of the mean; TCCD, 2,3,7,8-tetrachlorodibenzo-*p*-dioxin; WT, wild type.

and BaP, also failed to stimulate *Cyp1a1* transcript accumulation in liver tissue from AHR null rats (Figure S3). AHR null rats did not significantly differ from WT rats in an assortment of reproductive parameters (responsiveness to gonadotropins, fertility, or pregnancy-associated litter size; Figure 3E–G).

We observed two pregnancy-associated responses to TCDD (Figures 1 and 2). High concentrations of TCDD (20 μg/kg BW) resulted in pregnancy failure, whereas lower concentrations of TCDD (2 μg/kg BW) yielded placentation site adaptations. Fetal survival rate in dams treated with 20 μg/kg BW was significantly higher in AHR null animals (87.9%) than in WT animals (12.9%) and approximated the near 100% survival rate observed with oil-treated animals or those treated with the lower dose of TCDD (2 μg/kg BW). Both responses to TCDD were dependent upon AHR. Figure 4 shows the results of TCDD on pregnancy (Figure 4A), intrauterine trophoblast cell invasion, as assessed by immunolocalization of cytokeratin (Figure 4B,C), and the expression of invasive trophoblast cell-specific transcript *Prl7b1* (Figure 4D).

Evaluation of Placental Adaptations of CYP1A1 Null Rats Treated with Oil or TCDD

Given that CYP1A1 is a prominent downstream target of AHR signaling (Mimura and Fujii-Kuriyama 2003; Nebert et al. 1993; Whitlock 1999) and is capable of the biotransformation of biologically relevant endogenous and exogenous molecules (Shenoy et al. 2010; Stejskalova and Pavek 2011; Tsuchiya et al. 2005), we next evaluated a potential role for CYP1A1 in the TCDD-activated pregnancy phenotype and placental adaptations. A CYP1A1 null rat model was generated using CRISPR/Cas9 gene editing (Figure S4A). CYP1A1 heterozygote × CYP1A1 heterozygote breeding generated offspring with the expected Mendelian pattern of inheritance (Figure S4B). Homozygous CYP1A1 null rats did not possess detectable hepatic CYP1A1 protein (Figure S4C,D) nor did they exhibit hepatic CYP1A1 enzymatic activity (Figure S4E). We did not observe differences in fertility for CYP1A1 null rats vs. WT rats (Figure S4F). We investigated the effects of TCDD on pregnancy and placental adaptations. The presence of CYP1A1 did not significantly affect pregnancy responses or placental adaptations to the low dose of TCDD (Figure S5A–E).

Maternal AHR Signaling and TCDD-Activated Pregnancy Phenotypes

In the following experiments, we examined the importance of maternal AHR signaling in pregnancy-associated responses to TCDD. AHR null females were mated with WT males and compared with WT male × WT female intercrosses. Again, we tested the effects of low-dose TCDD (2 μg/kg BW) and high-dose TCDD (20 μg/kg BW) on pregnancy and placental adaptations. In contrast to the protective effects of the complete absence of AHR (Figure 4A), the maternal-only AHR deficiency was not protective for the high dose of TCDD (20 μg/kg BW), and, instead, there was increased pregnancy failure (Figure 4E), similar to the response to TCDD in the WT × WT pregnancies (Figure 4A). We also examined the role of maternal AHR signaling in mediating placental adaptations to the lower dose of TCDD (2 μg/kg BW). Interestingly, the absence of maternal AHR eliminated the TCDD-mediated increased endovascular trophoblast cell invasion (Figure 4F,G); however, a deficiency in embryonic/extraembryonic AHR signaling generated by establishing pregnancies from heterozygous females and *Ahr* null males did not compromise TCDD-induced intrauterine trophoblast cell invasion (Figure 4F,G).

RNA-Seq and Evaluation of the Uterine Mesometrial NK Cell Phenotype following TCDD Exposure

We next sought to determine where within the mother TCDD was acting to influence placental adaptations. We started our search at the metrial gland, the ultimate site of intrauterine endovascular trophoblast cell invasion. RNA-seq was performed on GD13.5 metrial gland tissues isolated from oil- and TCDD-treated females. Striking differences in the transcriptomic profiles were noted. Transcripts with an adjusted $p < 0.05$ were considered differentially regulated. We identified 312 up-regulated and

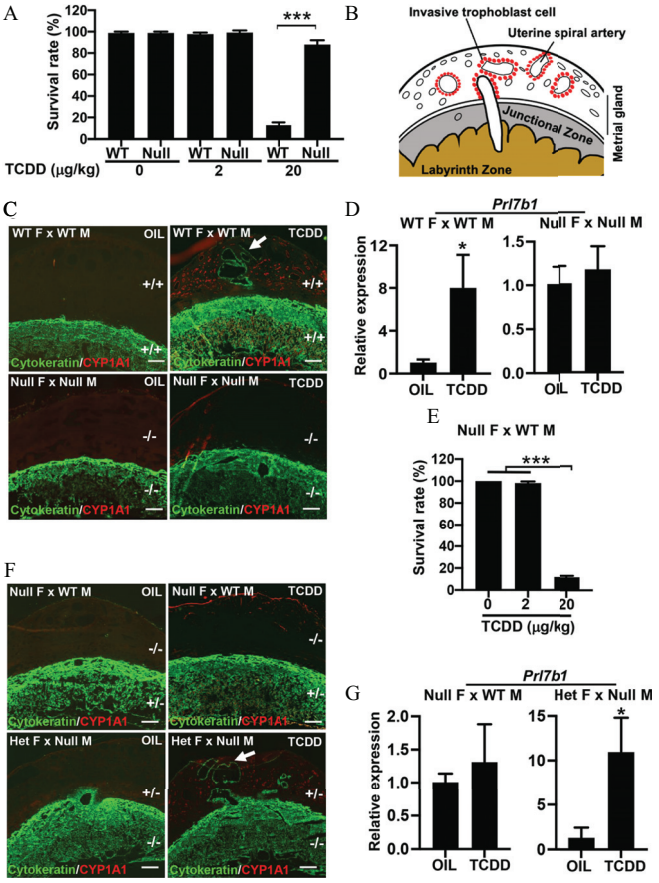

Figure 4. Evaluation of TCDD-activated placental adaptations resulting from mating WT (WT), AHR heterozygous, and AHR null rats. (A) Effect of low and high TCDD dose (2 µg/kg BW vs. 20 µg/kg weight) on WT and AHR null (Null) fetal survival rate ($n = 6$/group, *, $p < 0.0001$). Fetal survival rate was calculated on a per pregnancy basis as the number of live fetuses/total fetuses times 100. (B) Schematic of the rat placentation site. (C) Representative images from placentation sites of WT females (WT F) mated with WT males (WT M) or AHR null females (Null F) mated with AHR null males (Null M). Pregnant females treated with corn oil (OIL) or TCDD (2 µg/kg BW) at GD6.5 and euthanized on GD13.5. (D) Prl7b1 transcript abundance in GD13.5 metrial gland tissues isolated from WT F × WT M or Null F × Null M pregnancies treated with OIL ($n = 5$/group) or TCDD ($n = 6$/group; WT F × WT M, *, $p = 0.0043$). (E) Survival rate of embryos generated by crossing Null F × WT M ($n = 6$/group, *, $p < 0.0001$). (F) Representative images of placentation sites from Null F mated to WT M or *Ahr* heterozygous females (Het F) mated to Null M. Pregnant females were treated with OIL or TCDD (2 µg/kg BW) at GD6.5 and euthanized on GD13.5. Only placentation sites from null embryos (–/–) generated in the Het F × Null M pregnancies are presented. (G) Prl7b1 transcript abundance in GD13.5 metrial gland tissues isolated from Null F × WT M or from null placenta/fetal units (–/–) generated from Het F × Null M pregnancies treated with OIL ($n = 5$/group) or TCDD ($n = 6$/group); Het F × Null M, *, $p = 0.0043$. Null placenta/fetal units from the Het F × Null M mating were identified by genotyping fetal tissues. In (C) and (F), placentation sites were interrogated by pan-cytokeratin (green) and CYP1A1 (red) immunofluorescence. Genotypes of maternal and placental tissues are indicated: WT, +/+; Het, +/−; Null, –/–. White arrows show the depth of intrauterine endovascular trophoblast cell invasion. Scale bar: 500 µm. In (D) and (G), the delta-delta Ct method was used for relative quantification of gene expression for each sample normalized to 18S RNA. Data presented in (A) and (E) were analyzed using a one-way ANOVA followed by Tukey's multiple comparison post hoc test, whereas data presented in (D) and (G) were analyzed using the Wilcoxon rank sum test. Asterisks denote a statistically significant difference from the corresponding control. Bar graphs represent the mean ± SEM. The mean and SEM values for data presented in this figure are shown in Tables S15–S18. Note: AHR, aryl hydrocarbon receptor; ANOVA, analysis of variance; BW, body weight; cytokeratin, pan-cytokeratin; CYP1A1, cytochrome P450, family 1, subfamily a, polypeptide 1; F, female; GAPDH, glyceraldehyde 3-phosphate dehydrogenase; GD, gestation day; Het, heterozygous; M, male; Prl7b1, prolactin family 7, subfamily b, member 1; SEM, standard error of the mean; TCCD, 2,3,7,8-tetrachlorodibenzo-*p*-dioxin; WT, wild type.

581 down-regulated transcripts in oil vs. TCDD treatments (Figure 5A,B, C) (Excel Table S1). Among the TCDD–up-regulated transcripts, we observed classic AHR targets, such as *Cyp1a1*, and transcripts indicative of invasive trophoblast cells, such as *Prl5a1* and *Prl7b1* (Figure 5C). Conspicuous among the TCDD down-regulated transcripts were transcripts characteristic of NK cells (Figure 5C). The similarity of TCDD treatment (Figure 4) and NK cell deficiency (as reported previously by Chakraborty et al. 2011; Renaud et al. 2017) on intrauterine endovascular trophoblast cell invasion and the TCDD-mediated decrease in metrial gland NK cell-characteristic transcripts prompted further examination of the effects of TCDD on NK cells in the metrial gland. Distributions and numbers of NK cells within GD13.5 metrial glands of oil- and TCDD-treated rats were assessed by perforin immunohistochemistry and CD161-flow cytometry. The distribution or number of NK cells within the metrial gland of rats treated with TCDD did not significantly differ from those of rats treated with oil (Figure 5D,E). Some NK cell-associated transcripts were higher (*Klrd1, Ly49s3*), some did not differ in their expression (*Ly49s5, Gzmm*), whereas others were lower (*Klra5, Prf1, Gzmb*) (Figure 5F). The differentially regulated transcripts encode receptors mediating NK cell–target cell interactions (*Klrd1, Ly49s3, Klra5*) and components of the NK cell killing machinery (*Prf1, Gzmb*).

Measures of AHR Signaling at the Placentation Site of Rats Treated with TCDD or Oil

TCDD is a known agonist of the AHR signaling pathway (Bock 2018; Murray et al. 2014; Wilson and Safe 1998). CYP1A1 is a sensitive downstream target of TCDD activation of AHR signaling (Mimura and Fujii-Kuriyama 2003; Nebert et al. 1993; Whitlock 1999). Consequently, we examined CYP1A1 activation in the placentation site of oil- and TCDD-treated pregnant rats. CYP1A1 immunostaining revealed that AHR signaling was prominently activated in the metrial gland and in the labyrinth zone but not in the junctional zone of TCDD-treated pregnant rats [Figure 2B (oil); Figure 6A]. *Cyp1a1* transcript levels were also dramatically higher in the metrial gland and labyrinth zone of TCDD-treated pregnant rats (Figure 6B,C). Transcript levels for two other AHR downstream targets, *Cyp1b1* and *Ahrr* (Thackaberry et al. 2005; Watson et al. 2014), were also higher in the metrial gland and labyrinth zone (Figure 6B,C). CYP1A1 was not detectable in cytokeratin-positive trophoblast cells (Figure 6A) but did colocalize with endothelial cell-specific antigens recognized by antibodies to CD31 and RECA1 in the metrial gland and labyrinth zone (Figure 6D,E). We next examined the actions of TCDD on rat TS cells and rat arterial endothelial cells. Rat TS cells treated with TCDD did not differ significantly in *Cyp1a1* expression from control (Figure 6F); but rat arterial endothelial cells expressed significantly more *Cyp1a1* after TCDD treatment compared with the control (Figure 6G).

Evaluation of Immune and Endothelial Cell Phenotypes at the Uterine–Placental Interface in Rats Exposed to TCDD

The apparent phenotypic effects of TCDD on NK cells prompted a deeper examination of the responses of cellular constituents within the metrial gland (uterine–placental interface) from oil- and TCDD-treated pregnant females. scRNA-seq analysis was performed on GD13.5 metrial glands from oil- and TCDD-treated pregnant females. A total of the 48,863 cells met quality control standards (Figure 7A; Figure S6A–D) and resulted in the identification of six clusters with distinct expression profiles (Figure 7B–F; Figure S6E,F and Excel Table S2). Invasive trophoblast cells were not represented among the clusters owing to

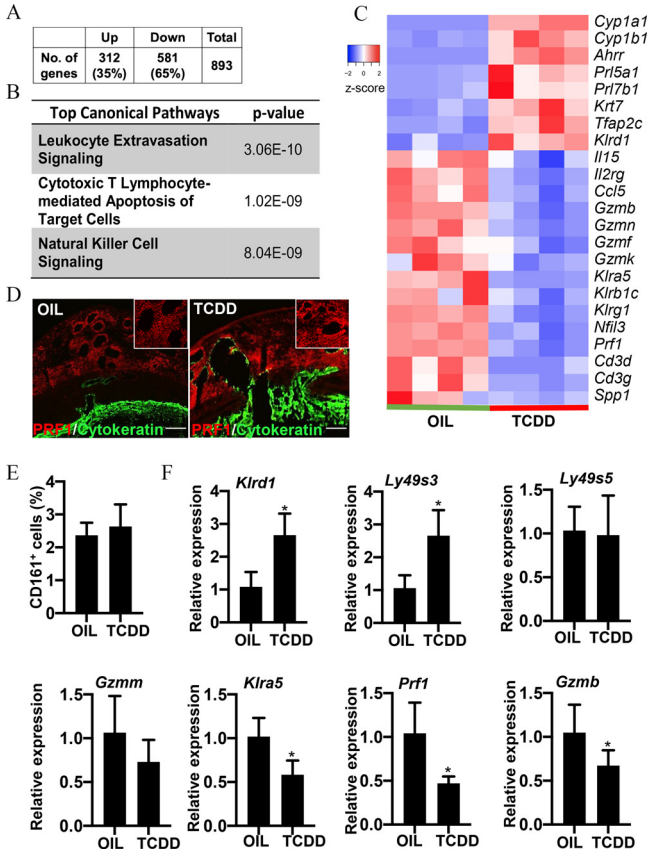

Figure 5. Effects of TCDD on metrial gland (uterine–placental interface) transcript profiles. Transcript profiles were determined by RNA-sequencing (RNA-seq) of metrial gland tissue obtained from pregnant rats treated with corn oil (OIL) or TCDD (2 μg/kg BW) at GD6.5 and harvested at GD13.5. The results are presented in a table (A) significantly upregulated and down-regulated transcripts in response to TCDD ($p < 0.05$ and $\log_2$-fold change either direction >1.5). (B) Gene ontology analysis of top dysregulated genes. (C) A heatmap showing select differentially expressed genes in replicates of OIL- and TCDD-treated rats. (D) Distribution of NK cells within GD13.5 metrial glands of OIL- or TCDD-treated rats assessed by perforin immunohistochemistry ($n = 3$/group). Scale bar: 500 μm. (E) NK cell numbers measured by CD161-flow cytometry ($n = 3$/group). (F) Validation of RNA-seq results by RT-qPCR ($n = 5$/group). The level of significance was determined using the Wilcoxon rank sum test (*Klrd1*, *, $p = 0.0079$; *Ly49s3c*; *Klra5*, *, $p = 0.0159$; *Prf1*, *, $p = 0.0079$; *Gzmb*, *, $p = 0.0079$). Transcript expression level is relative to control. The delta-delta Ct method was used for relative quantification of gene expression for each sample normalized to 18S RNA. Asterisks denote a statistically significant difference from the corresponding controls. Bar graphs represent the mean ± SEM. The mean and SEM values for data presented in this figure are shown in Tables S19 and S20. Note: BW, body weight; cytokeratin, pan-cytokeratin; down, down-regulation; GD, gestation day; Gzmb, granzyme B; Klra5, killer cell lectin-like receptor, subfamily a, member 5; Klrd1, killer cell lectin-like receptor subfamily D, member 1; Ly49s3c, Ly-49 stimulatory receptor 3; NK, natural killer; Prf1, perforin 1; RT-qPCR, real-time quantitative polymerase chain reaction; SEM, standard error of the mean; TCCD, 2,3,7,8-tetrachlorodibenzo-*p*-dioxin; up, up-regulation.

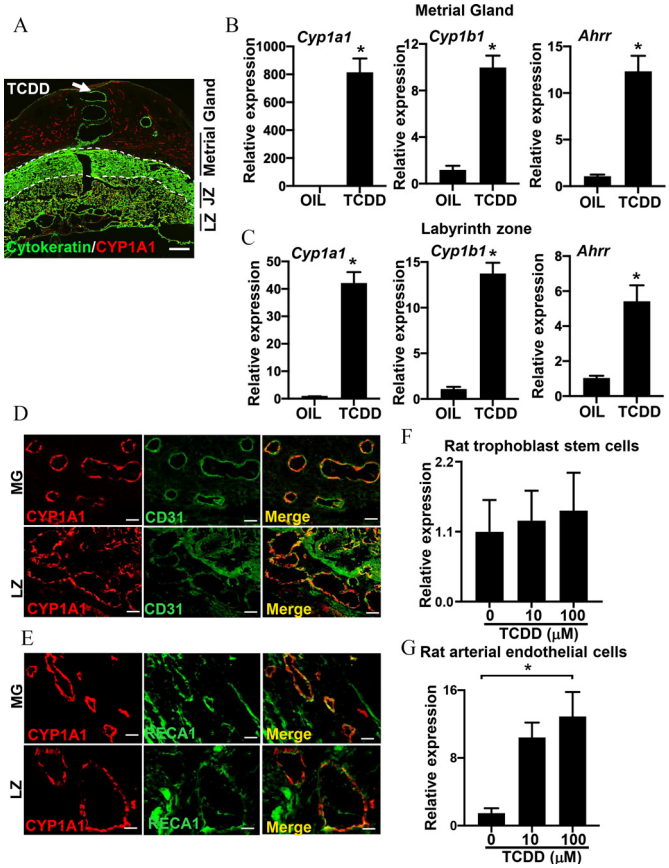

Figure 6. Evaluation of measures of AHR pathway activation in placentation sites of rats treated with oil or TCDD. (A) A representative image of pan-cytokeratin (green) and CYP1A1 (red) immunostaining of a GD13.5 placentation site from a pregnant female rat treated with TCDD (2 μg/kg BW) at GD6.5. Scale bar: 500 μm. Expression of *Cyp1a1*, *Cyp1b1*, and *Ahrr* in the GD13.5 (B) metrial gland or (C) labyrinth zone tissues from pregnant rats treated with corn oil (OIL) or TCDD (2 μg/kg BW) at GD6.5 ($n = 6$/group). Metrial gland: *Cyp1a1*, *, $p = 0.0079$; *Cyp1b1*, *, $p = 0.0079$; and *Ahrr*, *, $p = 0.0079$; labyrinth zone: *Cyp1a1*, *, $p = 0.0022$ and *Cyp1b1*, *, $p = 0.0022$; *Ahrr*, $p = 0.0022$. Asterisks denote a statistically significant difference from the corresponding control. Representative immunofluorescence images for (D) CD31 and CYP1A1 colocalization and (E) RECA1 and CYP1A1 colocalization in GD13.5 metrial gland and labyrinth zone tissues from pregnant rats treated with corn oil (OIL) or TCDD (2 μg/kg BW) at GD6.5. Scale bar: 50 μm. *Cyp1a1* expression in (F) rat trophoblast stem cells and (G) rat arterial endothelial cells following vehicle or TCDD treatment for 24 h ($n = 6$). *Cyp1a1* transcript levels were measured by RT-qPCR (*, $p < 0.0001$). Transcript expression level is relative to control. Data were analyzed using the Wilcoxon rank sum test (B and C) and an ANOVA followed by Tukey's multiple comparison post hoc test (F and G). Bar graphs represent the mean ± SEM. The mean and SEM values for data presented in this figure are shown in Tables S21–S24. Note: Ahrr, aryl-hydrocarbon receptor repressor; ANOVA, analysis of variance; BW, body weight; CD31, cluster of differentiation 31; Cyp1a1, cytochrome P450, family 1, subfamily a, polypeptide 1; Cyp1b1, cytochrome P450, family 1, subfamily b, polypeptide 1; GD, gestation day; JZ, junctional zone; LZ, labyrinth zone; MG, metrial gland; RECA1, Rat Endothelial Cell Antigen-1; RT-qPCR, real-time quantitative polymerase chain reaction; SEM, standard error of the mean; TCCD, 2,3,7,8-tetrachlorodibenzo-*p*-dioxin.

their limited numbers. We observed similarities in transcript profiles for bulk RNA-seq (Figure 5) and scRNA-seq (Figure 7).

Metrial gland scRNA-seq confirmed that intrauterine NK cells from TCDD-treated pregnant rats were distinct from intrauterine NK cells from oil-treated pregnant rats (Figure 7D). NK cells were defined by the expression of *Prf1, Nkg7, Xcl1,* various granzymes (Gzm), and killer cell lectin-like receptor (KLR) genes. A total of 6,940 NK cells were analyzed. TCDD treatment resulted in pronounced effects on transcripts characteristic of NK cells, including seven members of the killer cell lectin-like receptor family, as well as transcripts encoding other NK cell-specific surface proteins, and granule associated proteins (Excel Table S3). TCDD treatment also led to differential regulation of interferon inducible transcripts, transcripts for components of NK cell signaling pathways, and several transcripts for the class I histocompatibility complex (Excel Tables S3 and S4). NK cells did

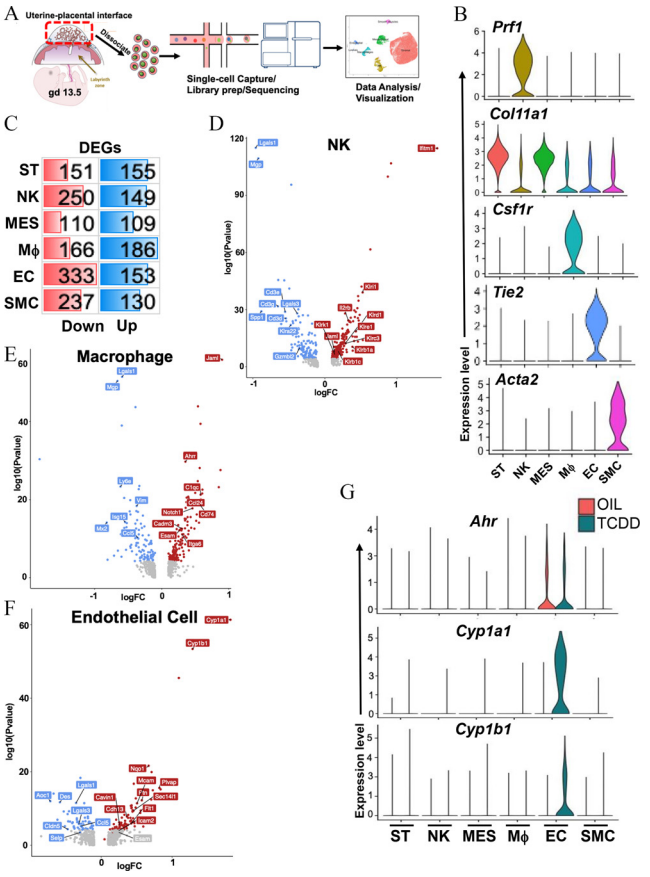

Figure 7. Mapping cell dynamics within the metrial gland (uterine–placental interface) of pregnancies exposed to oil or TCDD using scRNA-seq. Metrial glands were harvested on GD13.5 from pregnant rats treated with corn oil (OIL) or TCDD (2 μg/kg BW) at GD6.5 and analyzed by scRNA-seq. (A) A flow diagram illustrating the study design and analysis strategy. (B) Expression of canonical markers identifying cell clusters. (C) Number of differentially expressed genes (DEGs) following TCDD treatment in various cell clusters. Volcano plots showing DEGs between OIL and TCDD samples in (D) natural killer (NK) cells, (E), macrophages (Mϕ), and (F) endothelial cells (EC). Red dots represent up-regulated genes, whereas blue dots represent down-regulated genes. (G) Expression of *Ahr*, *Cyp1a1*, and *Cyp1b1* in stromal (ST) cells, NK cells, mesenchymal (MES) cells, Mϕ, EC, and smooth muscle cells (SMC). Data were analyzed by a two-sided Wilcoxon-rank-sum test, FDR <0.05, logFC >0.15. Additional lists of relevant differentially regulated transcripts and pathway analysis are provided in Excel Tables S2–S8. Note: Ahr, aryl hydrocarbon receptor; BW, body weight; Cyp1a1, cytochrome P450, family 1, subfamily a, polypeptide 1; Cyp1b1, cytochrome P450, family 1, subfamily b, polypeptide 1; down, down-regulation; FDR, false discovery rate; GD, gestation day; logFC, log fold change; scRNA-seq, single cell RNA sequencing; TCCD, 2,3,7,8-tetrachlorodibenzo-*p*-dioxin; up, up-regulation.

not exhibit detectable *Ahr* transcripts and TCDD did not activate known AHR target genes (e.g., *Cyp1a1*) (Figure 7G).

Macrophages were also affected by TCDD exposure. Macrophages were defined by the expression of *Cd74*, *Csf1r*, *C1qa*, *Lyz2*, and *Fcer1g*. TCDD-mediated differential macrophage transcript expression was observed for several members of the class I histocompatibility complex, cell adhesion molecules and extracellular matrix components, chemokines, and immune effector molecules (Figure 7E and Excel Tables S5 and S6). Macrophages exhibited minimal expression of *Ahr*, and TCDD treatment resulted in a modest activation of *Ahrr*, a known AHR target gene (Figure 7G).

Endothelial cells emerged as the primary target of TCDD action, consistent with the identification of CYP1A1 activation in endothelial cells of metrial glands from TCDD-treated pregnant females (Figure 6D,E). Endothelial cells were defined by the expression of *Plvap, Tie2, Cav1, Cavin2, Il33* and *Adgrl4*. Three classic AHR targets (*Cyp1a1*, *Cyp1b1*, *Nqo1*) were prominently activated in metrial gland endothelial cells following TCDD exposure (Figure 7F). This coincides with endothelial cells being the primary site of *Ahr* expression within the metrial gland (Figure 7G). TCDD affected endothelial cell expression of transcripts encoding proteins associated with extracellular matrix, cell–cell adhesion and cell migration, endothelial cell signaling, leukocyte development and trafficking, hemostasis, members of the class I histocompatibility complex, and interferon responsiveness (Excel Tables S7 and S8). We also identified transcripts establishing potential ligand–receptor signaling modules between endothelial cells and NK cells and between endothelial cells and macrophages (Excel Table S9).

Finally, we used scRNA-seq of PBMCs to determine whether TCDD treatment affected immune cells that enter the metrial gland. TCDD exposure (2 μg/kg BW) on GD6.5 did not have a detectable influence on the transcriptomes of circulating T cells, monocytes, B cells, or NK cells harvested on GD13.5 (Figure S7; Excel Tables S10–S14). These findings are consistent with our observations that TCDD-dependent phenotypes of immune cells within the metrial gland are secondary to TCDD actions on endothelial cells.

Discussion

Within our environment we are exposed to a diverse array of compounds affecting reproduction, including the biology of pregnancy (Crain et al. 2008; Fowler et al. 2012; Gingrich et al. 2020; Rattan et al. 2017). Among these environmental stressors are chemicals that impact physiological processes through activation of AHR, a ligand-driven transcriptional regulator (Beischlag et al. 2008; Gore et al. 2015; Schmidt and Bradfield 1996; Wilson and Safe 1998). In the present study, we examined the effects of an environmental pollutant, TCDD, representing a prototypical AHR ligand (Denison and Nagy 2003), on pregnancy and placentation in the rat. The actions of TCDD were dose dependent. High TCDD doses interfered with pregnancy, whereas low doses, capable of inducing both maternal and fetal AHR signaling, elicited placentation site-specific adaptations. Maternal, placental, and fetal responses to TCDD were contingent upon a functional AHR signaling system but not CYP1A1. Furthermore, TCDD-driven placental adaptations were dependent upon maternal AHR signaling. Within the uterine–placental interface, TCDD directly targeted uterine endothelial cells and indirectly modulated intrauterine immune cell and invasive trophoblast cell dynamics.

Mouse and rat *Ahr* mutant models exhibit phenotypic similarities and possibly some differences. Inactivation of AHR in both the mouse and rat interferes with responses to xenobiotic challenges (Fernandez-Salguero et al. 1995; Harrill et al. 2013, 2016; Mimura et al. 1997; Phadnis-Moghe et al. 2016; Schmidt et al. 1996). The mouse and rat may differ regarding the physiological consequences of disruption of their respective *Ahr* locus. Mouse vs. rat differences have been noted for the involvement of AHR in liver and kidney physiology/pathophysiology (Harrill et al. 2013). However, caution is required when evaluating the biology of global *Ahr* mutant mouse models. Developmental and reproductive phenotypes associated with the *Ahr* null mouse are not consistent among the reported models. Two *Ahr* null mouse models exhibited growth delays and reproductive anomalies (Fernandez-Salguero et al. 1995; Karman 2011; Schmidt et al. 1996), whereas a third *Ahr* null mouse model showed fertility similar to WT mice (Mimura et al. 1997). *Ahr* null rats resembled the latter mouse model, and were indistinguishable from WT rats in their breeding and in an assortment of parameters of

reproductive performance. Potential origins of phenotypic heterogeneity among *Ahr* mutant mouse models have been discussed (Hernández-Ochoa et al. 2009; Lahvis and Bradfield 1998). Our findings in the *Ahr* null rat highlight the need for caution in interpreting developmental and reproductive phenotypes previously ascribed to *Ahr* null mouse models.

The trophoblast cell is the parenchymal cell of the placenta (Georgiades et al. 2002; Knöfler et al. 2019; Maltepe and Fisher 2015; Soares et al. 2018). We observed activation of intrauterine trophoblast cell invasion following exposure to TCDD. Based on our results, rat trophoblast cells were not a direct target of TCDD action. Rat trophoblast cells developing within the placenta or in cell culture did not activate CYP1A1 expression when exposed to TCDD or other AHR activators. There are cells within the rodent placentation site that respond to TCDD but not trophoblast cells. This is in stark contrast to human trophoblast cells, which exhibit a striking response to TCDD and other AHR activators (Stejskalova and Pavek 2011; Stejskalova et al. 2011). AHR expression is readily detected in the human placenta within trophoblast and some non-trophoblast cell types (Jiang et al. 2010; Stejskalova et al. 2011), whereas efforts to localize AHR expression in the rodent placenta are subject to debate. AHR expression is low in the rat placenta relative to other tissues (Carver et al. 1994). Within the rat placenta, AHR appears to be more abundant in the labyrinth zone than the junctional zone (Ishimura et al. 2002). Evidence of syncytiotrophoblast and non-trophoblast cell AHR expression has been reported (Detmar et al. 2008; Kitajima et al. 2004; Stejskalova et al. 2011). Species differences in trophoblast cell AHR signaling are an important consideration in using rodents for modeling environmental exposures on human placental health. Molecular mechanisms that underlie differences in rodent vs. human trophoblast cell responsiveness to TCDD are unknown as is the evolutionary significance of such species-specific cellular responses.

Pregnancy-dependent biological responses were influenced by TCDD dosage. High doses of TCDD resulted in pregnancy failure. These adverse TCDD actions may be a direct consequence of disruptions in maternal to fetal nutrient delivery. AHR activation has been shown to disrupt vascularization of the labyrinth zone of the rat placenta (Ishimura et al. 2006, 2009; Wu et al. 2014), which is the main conduit for maternal–fetal nutrient transfer (Burton and Fowden 2012; Knipp et al. 1999). Exposure to low-dose TCDD yielded a pregnancy-specific adaptive response characterized by activation of intrauterine endovascular trophoblast cell invasion. The response is notable in that the lining of uterine spiral arterioles changes from endothelial cells to trophoblast cells, along with putative differences in the properties of cells lining the vessels, including permeability, coagulation, injury repair, immune and inflammatory cell regulation, intra-arterial cell–cell regulation, and/or responses to physiological and pathological perturbations. Enhanced trophoblast-guided uterine spiral artery remodeling supports nutrient delivery for fetal growth (Kaufmann et al. 2003; Pollheimer et al. 2018). Activation of endovascular trophoblast cell invasion is also observed with two other *in vivo* manipulations: *a*) hypoxia and *b*) NK cell depletion. Hypoxia (Rosario et al. 2008), NK cell depletion (Chakraborty et al. 2011; Renaud et al. 2017), and, based on our findings, TCDD exposure each resulted in an activation of intrauterine endovascular trophoblast cell invasion. How these triggers operate to increase trophoblast cell invasion is not known. Current evidence indicates that hypoxia triggers trophoblast progenitor cell differentiation to the invasive trophoblast cell lineage (Chakraborty et al. 2011, 2016; Chang et al. 2018; Soares et al. 2017; Wakeland et al. 2017), whereas the absence of NK cells impairs uterine spiral artery remodeling, which decreases oxygen tension at the uterine interface leading to trophoblast invasion (Chakraborty et al. 2011) . The involvement of hypoxia and/or NK cells in TCDD activation of endovascular trophoblast cell invasion is unknown. It is an interesting coincidence that the biologically active state of both hypoxia-inducible factor and AHR requires physical interactions with ARNT (McIntosh et al. 2010).

Based on the results of our study, we conclude that the actions of TCDD on placental adaptations required a functional AHR signaling pathway in the mother but not in the placenta or fetus. TCDD failed to elicit an adaptive response in pregnant AHR null rats mated to WT males. In order to begin to understand how TCDD was acting, we focused our attention at the uterine–placental interface, a structure also referred to as the metrial gland (Selye and McKeown 1934). This uterine compartment is immediately adjacent to the developing placenta, the site of vasculature supplying the placenta and a unique leukocytic cell composition, and the ultimate destination of invasive trophoblast cells (Soares et al. 2012). The distribution of NK cells and invasive trophoblast cells exhibit a reciprocal relationship. NK cells are abundant at the uterine interface as the placenta is being established and then vacate the region as trophoblast cells invade the uterine parenchyma (Ain et al. 2003). The transcriptomes of both immune and nonimmune cells within the uterine–placental interface were affected by TCDD. However, immunohistochemical and scRNA-seq analyses for CYP1A1 and AHR expression demonstrated that endothelial cells were the predominant direct cellular site of TCDD action at the uterine–placental interface. Endothelial cells have been previously shown to be responsive to AHR activation (Dauchy et al. 2009; Stegeman et al. 1995). Thus, TCDD effects on other cellular constituents at the uterine–placental interface were indirect. The scRNA-seq analysis supports endothelial cells serving as a TCDD/AHR-regulated gatekeeper controlling immune cell entry into the uterus (Reglero-Real et al. 2016; Wettschureck et al. 2019) through the production of cytokines/chemokines regulating intrauterine immune cell phenotypes (Al-Soudi et al. 2017; Pober and Sessa 2007; Sturtzel 2017) or, alternatively, by facilitating trophoblast cell–endothelial cell interactions prerequisite for endovascular invasive trophoblast cell migration and uterine spiral artery remodeling (Harris et al. 2009; Sato 2020). Thus, endothelial cells emerge as a key mediator of a pathophysiologic response to an environmental exposure.

Comparison of rat and human TCDD exposures during pregnancy may not be optimal and our experiments investigating the effects of TCDD on rat placentation may be of limited value for predicting human risk assessments (Emond et al. 2004, 2016; Hurst et al. 1998, 2000). However, our findings demonstrate the potential for TCDD, and possibly other AHR ligands, to act as a modulator(s) of placental development. Furthermore, they highlight the need to consider a role for AHR signaling and the impact of environmental exposures on cellular dynamics at the human uterine–placental interface.

Acknowledgments

We thank L. Robertson for advice and S. Oxley and B. Miller for their assistance. The research was supported by grants from the National Institutes of Health (HD020676, ES028957, ES029280) and an American Heart Association postdoctoral fellowship (K.K.).

References

Ain R, Canham LN, Soares MJ. 2003. Gestation stage-dependent intrauterine trophoblast cell invasion in the rat and mouse: novel endocrine phenotype and regulation. Dev Biol 260(1):176–190, PMID: 12885563, https://doi.org/10.1016/S0012-1606(03)00210-0.

Ain R, Konno T, Canham LN, Soares MJ. 2006. Phenotypic analysis of the rat placenta. Methods Mol Med 121:295–313, PMID: 16251750, https://doi.org/10.1385/1-59259-983-4:293.

Al-Soudi A, Kaaij MH, Tas SW. 2017. Endothelial cells: from innocent bystanders to active participants in immune responses. Autoimmun Rev 16(9):951–962, PMID: 28698091, https://doi.org/10.1016/j.autrev.2017.07.008.

Asanoma K, Rumi MAK, Kent LN, Chakraborty D, Renaud SJ, Wake N, et al. 2011. FGF4-dependent stem cells derived from rat blastocysts differentiate along the trophoblast lineage. Dev Biol 351(1):110–119, PMID: 21215265, https://doi.org/10.1016/j.ydbio.2010.12.038.

Avilla MN, Malecki KMC, Hahn ME, Wilson RH, Bradfield CA. 2020. The Ah receptor: adaptive metabolism, ligand diversity, and the xenokine model. Chem Res Toxicol 33(4):860–879, PMID: 32259433, https://doi.org/10.1021/acs.chemrestox.9b00476.

Beischlag TV, Luis Morales J, Hollingshead BD, Perdew GH. 2008. The aryl hydrocarbon receptor complex and the control of gene expression. Crit Rev Eukaryot Gene Expr 18(3):207–250, PMID: 18540824, https://doi.org/10.1615/critreveukargeneexpr.v18.i3.20.

Bergman Å, Heindel JJ, Jobling S, Kidd KA, Zoeller RT. 2013. *State of the Science of Endocrine Disrupting Chemicals - 2012*. Geneva, Switzerland: United Nations Environment Programme and the World Health Organization. https://apps.who.int/iris/bitstream/handle/10665/78101/9789241505031_eng.pdf?sequence=1&isAllowed=y (accessed 5 October 21).

Birnbaum LS. 1994. The mechanism of dioxin toxicity: relationship to risk assessment. Environ Health Perspect 102(suppl 9):157–167, PMID: 7698077, https://doi.org/10.1289/ehp.94102s9157.

Bock KW. 2018. From TCDD-mediated toxicity to searches of physiologic AHR functions. Biochem Pharmacol 155:419–424, PMID: 30055148, https://doi.org/10.1016/j.bcp.2018.07.032.

Brosens I, Pijnenborg R, Vercruysse L, Romero R. 2011. The "great obstetrical syndromes" are associated with disorders of deep placentation. Am J Obstet Gynecol 204(3):193–201, PMID: 21094932, https://doi.org/10.1016/j.ajog.2010.08.009.

Brosens I, Puttemans P, Benagiano G. 2019. Placental bed research: I. The placental bed: from spiral arteries remodeling to the great obstetrical syndromes. Am J Obstet Gynecol 221(5):437–456, PMID: 31163132, https://doi.org/10.1016/j.ajog.2019.05.044.

Burns KA, Zorrilla LM, Hamilton KJ, Reed CE, Birnbaum LS, Korach KS. 2013. A single gestational exposure to 2,3,7,8-tetrachlorodibenzo-*p*-dioxin disrupts the adult uterine response to estradiol in mice. Toxicol Sci 136(2):514–526, PMID: 24052564, https://doi.org/10.1093/toxsci/kft208.

Burton GJ, Fowden AL. 2012. The placenta and developmental programming: balancing fetal nutrient demands with maternal resource allocation. Placenta 33(suppl):S23–S27, PMID: 22154688, https://doi.org/10.1016/j.placenta.2011.11.013.

Burton GJ, Fowden AL, Thornburg KL. 2016. Placental origins of chronic disease. Physiol Rev 96(4):1509–1565, PMID: 27604528, https://doi.org/10.1152/physrev.00029.2015.

Carver LA, Hogenesch JB, Bradfield CA. 1994. Tissue specific expression of the rat Ah-receptor and ARNT mRNAs. Nucleic Acids Res 22(15):3038–3044, PMID: 8065918, https://doi.org/10.1093/nar/22.15.3038.

Chakraborty D, Cui W, Rosario GX, Scott RL, Dhakal P, Renaud SJ, et al. 2016. HIF-KDM3A-MMP12 regulatory circuit ensures trophoblast plasticity and placental adaptations to hypoxia. Proc Natl Acad Sci USA 113(46):E7212–E7221, PMID: 27807143, https://doi.org/10.1073/pnas.1612626113.

Chakraborty D, Rumi MAK, Konno T, Soares MJ. 2011. Natural killer cells direct hemochorial placentation by regulating hypoxia-inducible factor dependent trophoblast lineage decisions. Proc Natl Acad Sci USA 108(39):16295–16300, PMID: 21900602, https://doi.org/10.1073/pnas.1109478108.

Chang C-W, Wakeland AK, Parast MM. 2018. Trophoblast lineage specification, differentiation and their regulation by oxygen tension. J Endocrinol 236(1):R43–R56, PMID: 29259074, https://doi.org/10.1530/JOE-17-0402.

Crain DA, Janssen SJ, Edwards TM, Heindel J, Ho S-m, Hunt P, et al. 2008. Female reproductive disorders: the roles of endocrine-disrupting compounds and developmental timing. Fertil Steril 90(4):911–940, PMID: 18929049, https://doi.org/10.1016/j.fertnstert.2008.08.067.

Dauchy S, Miller F, Couraud P-O, Weaver RJ, Weksler B, Romero I-A, et al. 2009. Expression and transcriptional regulation of ABC transporters and cytochromes P450 in hCMEC/D3 human cerebral microvascular endothelial cells. Biochem Pharmacol 77(5):897–909, PMID: 19041851, https://doi.org/10.1016/j.bcp.2008.11.001.

Denison MS, Nagy SR. 2003. Activation of the aryl hydrocarbon receptor by structurally diverse exogenous and endogenous chemicals. Annu Rev Pharmacol Toxicol 43:309–334, PMID: 12540743, https://doi.org/10.1146/annurev.pharmtox.43.100901.135828.

Detmar J, Rennie MY, Whiteley KJ, Qu D, Taniuchi Y, Shang X, et al. 2008. Fetal growth restriction triggered by polycyclic aromatic hydrocarbons is associated with altered placental vasculature and *AhR*-dependent changes in cell death. Am J Physiol Endocrinol Metab 295(2):E519–E530, PMID: 18559983, https://doi.org/10.1152/ajpendo.90436.2008.

Dietrich C, Kaina B. 2010. The aryl hydrocarbon receptor (AhR) in the regulation of cell–cell contact and tumor growth. Carcinogenesis 31(8):1319–1328, PMID: 20106901, https://doi.org/10.1093/carcin/bgq028.

Efremova M, Vento-Tormo R. 2021. Inference of ligand–receptor pairs from single-cell transcriptomics data. Methods Mol Biol 2346:1–10.

Emond C, Birnbaum LS, DeVito MJ. 2004. Physiologically based pharmacokinetic model for developmental exposures to TCDD in the rat. Toxicol Sci 80(1):115–133, PMID: 15056810, https://doi.org/10.1093/toxsci/kfh117.

Emond C, DeVito M, Warner M, Eskenazi B, Mocarelli P, Birnbaum LS. 2016. An assessment of dioxin exposure across gestation and lactation using a PBPK model and new data from Seveso. Environ Int 92–93:23–32, PMID: 27045706, https://doi.org/10.1016/j.envint.2016.03.015.

Fernandez-Salguero P, Pineau T, Hilbert DM, McPhail T, Lee SS, Kimura S, et al. 1995. Immune system impairment and hepatic fibrosis in mice lacking the dioxin-binding Ah receptor. Science 268(5211):722–726, PMID: 7732381, https://doi.org/10.1126/science.7732381.

Fowler PA, Bellingham M, Sinclair KD, Evans NP, Pocar P, Fischer B, et al. 2012. Impact of endocrine-disrupting compounds (EDCs) on female reproductive health. Mol Cell Endocrinol 355(2):231–239, PMID: 22061620, https://doi.org/10.1016/j.mce.2011.10.021.

Georgiades P, Ferguson-Smith AC, Burton GJ. 2002. Comparative developmental anatomy of the murine and human definitive placentae. Placenta 23(1):3–19, PMID: 11869088, https://doi.org/10.1053/plac.2001.0738.

Gingrich J, Ticiani E, Veiga-Lopez A. 2020. Placenta disrupted: endocrine disrupting chemicals and pregnancy. Trends Endocrinol Metab 31(7):508–524, PMID: 32249015, https://doi.org/10.1016/j.tem.2020.03.003.

Gore AC, Chappell VA, Fenton SE, Flaws JA, Nadal A, Prins GS, et al. 2015. EDC-2: the Endocrine Society's second Scientific Statement on endocrine-disrupting chemicals. Endocr Rev 36(6):E1–E150, PMID: 26544531, https://doi.org/10.1210/er.2015-1010.

Gray LE, Wolf C, Mann P, Ostby JS. 1997. *In utero* exposure to low doses of 2,3,7,8-tetrachlorodibenzo-*p*-dioxin alters reproductive development of female Long Evans hooded rat offspring. Toxicol Appl Pharmacol 146(2):237–244, PMID: 9344891, https://doi.org/10.1006/taap.1997.8222.

Gu YZ, Hogenesch JB, Bradfield CA. 2000. The PAS superfamily: sensors of environmental and developmental signals. Annu Rev Pharmacol Toxicol 40:519–561, PMID: 10836146, https://doi.org/10.1146/annurev.pharmtox.40.1.519.

Harrill JA, Hukkanen RR, Lawson M, Martin G, Gilger B, Soldatow V, et al. 2013. Knockout of the aryl hydrocarbon receptor results in distinct hepatic and renal phenotypes in rats and mice. Toxicol Appl Pharmacol 272(2):503–518, PMID: 23859880, https://doi.org/10.1016/j.taap.2013.06.024.

Harrill JA, Layko D, Nyska A, Hukkanen RR, Manno RA, Grassetti A, et al. 2016. Aryl hydrocarbon receptor knockout rats are insensitive to the pathological effects of repeated oral exposure to 2,3,7,8-tetrachlorodibenzo-*p*-dioxin. J Appl Toxicol 36(6):802–814, PMID: 26278112, https://doi.org/10.1002/jat.3211.

Harris LK, Jones CJP, Aplin JD. 2009. Adhesion molecules in human trophoblast—a review. II. Extravillous trophoblast. Placenta 30(4):299–304, PMID: 19131105, https://doi.org/10.1016/j.placenta.2008.12.003.

Heindel JJ. 2019. The developmental basis of disease: update on environmental exposures and animal models. Basic Clin Pharmacol Toxicol 125(suppl 3):5–13, PMID: 30265444, https://doi.org/10.1111/bcpt.13118.

Hernández-Ochoa I, Karman BN, Flaws JA. 2009. The role of the aryl hydrocarbon receptor in the female reproductive system. Biochem Pharmacol 77(4):547–559, PMID: 18977336, https://doi.org/10.1016/j.bcp.2008.09.037.

Hurst CH, Abbott BD, DeVito MJ, Birnbaum LS. 1998. 2,3,7,8-Tetrachlorodibenzo-*p*-dioxin in pregnant Long Evans rats: disposition to maternal and embryo/fetal tissues. Toxicol Sci 45(2):129–136, PMID: 9848119, https://doi.org/10.1006/toxs.1998.2520.

Hurst CH, DeVito MJ, Setzer RW, Birnbaum LS. 2000. Acute administration of 2,3,7,8-tetrachlorodibenzo-*p*-dioxin (TCDD) in pregnant Long Evans rats: association of measured tissue concentrations with developmental effects. Toxicol Sci 53(2):411–420, PMID: 10696789, https://doi.org/10.1093/toxsci/53.2.411.

Iqbal K, Barg-Kues B, Broll S, Bode J, Niemann H, Kues W. 2009. Cytoplasmic injection of circular plasmids allows targeted expression in mammalian embryos. Biotechniques 47(5):959–968, PMID: 20041849, https://doi.org/10.2144/000113270.

Iqbal K, Dhakal P, Pierce SH, Soares MJ. 2021. Catechol-O-methyltransferase and pregnancy outcome: an appraisal in rat. Reprod Sci 28(2):462–469, PMID: 33048315, https://doi.org/10.1007/s43032-020-00348-7.

Iqbal K, Tran DA, Li AX, Warden C, Bai AY, Singh P, et al. 2015. Deleterious effects of endocrine disruptors are corrected in the mammalian germline by epigenome reprogramming. Genome Biol 16(1):59, PMID: 25853433, https://doi.org/10.1186/s13059-015-0619-z.

Ishimura R, Kawakami T, Ohsako S, Nohara K, Tohyama C. 2006. Suppressive effect of 2,3,7,8-tetrachlorodibenzo-*p*-dioxin on vascular remodeling that takes place in the normal labyrinth zone of rat placenta during late gestation. Toxicol Sci 91(1):265–274, PMID: 16495355, https://doi.org/10.1093/toxsci/kfj138.

Ishimura R, Kawakami T, Ohsako S, Tohyama C. 2009. Dioxin-induced toxicity on vascular remodeling of the placenta. Biochem Pharmacol 77(4):660–669, PMID: 19027717, https://doi.org/10.1016/j.bcp.2008.10.030.

Ishimura R, Ohsako S, Miyabara Y, Sakaue M, Kawakami T, Aoki Y, et al. 2002. Increased glycogen content and glucose transporter 3 mRNA level in the placenta of Holtzman rats after exposure to 2,3,7,8-tetrachlorodibenzo-*p*-dioxin. Toxicol Appl Pharmacol 178(3):161–171, PMID: 11858732, https://doi.org/10.1006/taap.2001.9333.

Jiang Y-z, Wang K, Fang R, Zheng J. 2010. Expression of aryl hydrocarbon receptor in human placentas and fetal tissues. J Histochem Cytochem 58(8):679–685, PMID: 20354149, https://doi.org/10.1369/jhc.2010.955955.

Jirtle RL, Skinner MK. 2007. Environmental epigenomics and disease susceptibility. Nat Rev Genet 8(4):253–262, PMID: 17363974, https://doi.org/10.1038/nrg2045.

Kaneko T. 2017a. Genome editing in mouse and rat by electroporation. Methods Mol Biol 1630:81–89, PMID: 28643251, https://doi.org/10.1007/978-1-4939-7128-2_7.

Kaneko T. 2017b. Genome editing of rat. Methods Mol Biol 1630:101–108, PMID: 28643253, https://doi.org/10.1007/978-1-4939-7128-2_9.

Kang E-R, Iqbal K, Tran DA, Rivas GE, Singh P, Pfeifer GP, et al. 2011. Effects of endocrine disruptors on imprinted gene expression in the mouse embryo. Epigenetics 6(7):937–950, PMID: 21636974, https://doi.org/10.4161/epi.6.7.16067.

Karman BN, Hernández-Ochoa I, Ziv-Gal A, Flaws JA. 2011. Involvement of the AHR in development and functioning of the female and male reproductive systems. In: *The AH Receptor in Biology and Toxicology*. Pohjanvirta R., ed. New York, NY: John Wiley and Sons, 437–466.

Kaufmann P, Black S, Huppertz B. 2003. Endovascular trophoblast invasion: implications for the pathogenesis of intrauterine growth retardation and preeclampsia. Biol Reprod 69(1):1–7, PMID: 12620937, https://doi.org/10.1095/biolreprod.102.014977.

Kitajima M, Khan KN, Fujishita A, Masuzaki H, Koji T, Ishimaru T. 2004. Expression of the arylhydrocarbon receptor in the peri-implantation period of the mouse uterus and the impact of dioxin on mouse implantation. Arch Histol Cytol 67(5):465–474, PMID: 15781987, https://doi.org/10.1679/aohc.67.465.

Knights KM, Stresser DM, Miners JO, Crespi CL. 2016. In vitro drug metabolism using liver microsomes. Curr Protoc Pharmacol 74:7.8.1–7.8.24, PMID: 27636111, https://doi.org/10.1002/cpph.9.

Knipp GT, Audus KL, Soares MJ. 1999. Nutrient transport across the placenta. Adv Drug Deliv Rev 38(1):41–58, PMID: 10837745, https://doi.org/10.1016/S0169-409X(99)00005-8.

Knöfler M, Haider S, Saleh L, Pollheimer J, Gamage T, James J. 2019. Human placenta and trophoblast development: key molecular mechanisms and model systems. Cell Mol Life Sci 76(18):3479–3496, PMID: 31049600, https://doi.org/10.1007/s00018-019-03104-6.

Knutson JC, Poland A. 1980. 2,3,7,8-Tetrachlorodibenzo-*p*-dioxin: failure to demonstrate toxicity in twenty-three cultured cell types. Toxicol Appl Pharmacol 54(3):377–383, PMID: 7394793, https://doi.org/10.1016/0041-008X(80)90163-5.

Konno T, Rempel LA, Arroyo JA, Soares MJ. 2007. Pregnancy in the brown Norway rat: a model for investigating the genetics of placentation. Biol Reprod 76(4):709–718, PMID: 17202390, https://doi.org/10.1095/biolreprod.106.056481.

Kransler KM, McGarrigle BP, Olson JR. 2007. Comparative developmental toxicity of 2,3,7,8-tetrachlorodibenzo-*p*-dioxin in the hamster, rat and guinea pig. Toxicology 229(3):214–225, PMID: 17126467, https://doi.org/10.1016/j.tox.2006.10.019.

La Merrill MA, Vandenberg LN, Smith MT, Goodson W, Browne P, Patisaul HB, et al. 2020. Consensus on the key characteristics of endocrine-disrupting chemicals as a basis for hazard identification. Nat Rev Endocrinol 16(1):45–57, PMID: 31719706, https://doi.org/10.1038/s41574-019-0273-8.

Lahvis GP, Bradfield CA. 1998. *Ahr* null alleles: distinctive or different? Biochem Pharmacol 56(7):781–787, PMID: 9774139, https://doi.org/10.1016/S0006-2952(98)00134-8.

Maltepe E, Fisher SJ. 2015. Placenta: the forgotten organ. Annu Rev Cell Dev Biol 31:523–552, PMID: 26443191, https://doi.org/10.1146/annurev-cellbio-100814-125620.

McIntosh BE, Hogenesch JB, Bradfield CA. 2010. Mammalian Per-Arnt-Sim proteins in environmental adaptation. Annu Rev Physiol 72:625–645, PMID: 20148691, https://doi.org/10.1146/annurev-physiol-021909-135922.

McMillan BJ, Bradfield CA. 2007. The aryl hydrocarbon receptor *sans* xenobiotics: endogenous function in genetic model systems. Mol Pharmacol 72(3):487–498, PMID: 17535977, https://doi.org/10.1124/mol.107.037259.

Mimura J, Fujii-Kuriyama Y. 2003. Functional role of AhR in the expression of toxic effects by TCDD. Biochim Biophys Acta 1619(3):263–268, PMID: 12573486, https://doi.org/10.1016/S0304-4165(02)00485-3.

Mimura J, Yamashita K, Nakamura K, Morita M, Takagi TN, Nakao K, et al. 1997. Loss of teratogenic response to 2,3,7,8-tetrachlorodibenzo-*p*-dioxin (TCDD) in mice lacking the Ah (dioxin) receptor. Genes Cells 2(10):645–654, PMID: 9427285, https://doi.org/10.1046/j.1365-2443.1997.1490345.x.

Mulero-Navarro S, Fernandez-Salguero PM. 2016. New trends in aryl hydrocarbon receptor biology. Front Cell Dev Biol 4:45, PMID: 27243009, https://doi.org/10.3389/fcell.2016.00045.

Murray IA, Patterson AD, Perdew GH. 2014. Aryl hydrocarbon receptor ligands in cancer: friend and foe. Nat Rev Cancer 14(12):801–814, PMID: 25568920, https://doi.org/10.1038/nrc3846.

Nebert DW, Puga A, Vasiliou V. 1993. Role of the Ah receptor and the dioxin-inducible [*Ah*] gene battery in toxicity, cancer, and signal transduction. Ann NY Acad Sci 685:624–640, PMID: 8395783, https://doi.org/10.1111/j.1749-6632.1993.tb35928.x.

Petrulis JR, Perdew GH. 2002. The role of chaperone proteins in the aryl hydrocarbon receptor core complex. Chem Biol Interact 141(1–2):25–40, PMID: 12213383, https://doi.org/10.1016/S0009-2797(02)00064-9.

Phadnis-Moghe AS, Chen W, Li J, Crawford RB, Bach A, D'Ingillo S, et al. 2016. Immunological characterization of the aryl hydrocarbon receptor (AHR) knockout rat in the presence and absence of 2,3,7,8-tetrachlorodibenzo-*p*-dioxin (TCDD). Toxicology 368–369:172–182, PMID: 27590929, https://doi.org/10.1016/j.tox.2016.08.019.

Pijnenborg R, Vercruysse L. 2010. Animal models of deep trophoblast invasion. In: *Placental Bed Disorders: Basic Science and Its Translation to Obstetrics*. Pijnenborg R, Brosens I, Romero R, eds. Cambridge, UK: Cambridge University Press, 127–139.

Pober JS, Sessa WC. 2007. Evolving functions of endothelial cells in inflammation. Nat Rev Immunol 7(10):803–815, PMID: 17893694, https://doi.org/10.1038/nri2171.

Poland A, Knutson JC. 1982. 2,3,7,8-Tetrachlorodibenzo-*p*-dioxin and related halogenated aromatic hydrocarbons: examination of the mechanism of toxicity. Annu Rev Pharmacol Toxicol 22:517–554, PMID: 6282188, https://doi.org/10.1146/annurev.pa.22.040182.002505.

Pollheimer J, Vondra S, Baltayeva J, Beristain AG, Knöfler M. 2018. Regulation of placental extravillous trophoblasts by the maternal uterine environment. Front Immunol 13(9):2597, PMID: 30483261, https://doi.org/10.3389/fimmu.2018.02597.

Ramadoss P, Marcus C, Perdew GH. 2005. Role of the aryl hydrocarbon receptor in drug metabolism. Expert Opin Drug Metab Toxicol 1(1):9–21, PMID: 16922649, https://doi.org/10.1517/17425255.1.1.9.

Rattan S, Zhou C, Chiang C, Mahalingam S, Brehm E, Flaws JA. 2017. Exposure to endocrine disruptors during adulthood: consequences for female fertility. J Endocrinol 233(3):R109–R129, PMID: 28356401, https://doi.org/10.1530/JOE-17-0023.

Reglero-Real N, García-Weber D, Millán J. 2016. Cellular barriers after extravasation: leukocyte interactions with polarized epithelia in the inflamed tissue. Mediators Inflamm 2016:7650260, PMID: 26941485, https://doi.org/10.1155/2016/7650260.

Renaud SJ, Scott RL, Chakraborty D, Rumi MAK, Soares MJ. 2017. Natural killer-cell deficiency alters placental development in rats. Biol Reprod 96(1):145–158, PMID: 28395334, https://doi.org/10.1095/biolreprod.116.142752.

Rissman EF, Adli M. 2014. Minireview: transgenerational epigenetic inheritance: focus on endocrine disrupting compounds. Endocrinology 155(8):2770–2780, PMID: 24885575, https://doi.org/10.1210/en.2014-1123.

Rosario GX, Konno T, Soares MJ. 2008. Maternal hypoxia activates endovascular trophoblast cell invasion. Dev Biol 314(2):362–375, PMID: 18199431, https://doi.org/10.1016/j.ydbio.2007.12.007.

Sato Y. 2020. Endovascular trophoblast and spiral artery remodeling. Mol Cell Endocrinol 503:110699, PMID: 31899258, https://doi.org/10.1016/j.mce.2019.110699.

Schmidt JV, Bradfield CA. 1996. Ah receptor signaling pathways. Annu Rev Cell Dev Biol 12:55–89, PMID: 8970722, https://doi.org/10.1146/annurev.cellbio.12.1.55.

Schmidt JV, Su GH, Reddy JK, Simon MC, Bradfield CA. 1996. Characterization of a murine Ahr null allele: involvement of the Ah receptor in hepatic growth and development. Proc Natl Acad Sci USA 93(13):6731–6736, PMID: 8692887, https://doi.org/10.1073/pnas.93.13.6731.

Schug TT, Janesick A, Blumberg B, Heindel JJ. 2011. Endocrine disrupting chemicals and disease susceptibility. J Steroid Biochem Mol Biol 127(3–5):204–215, PMID: 21899826, https://doi.org/10.1016/j.jsbmb.2011.08.007.

Selye H, McKeown T. 1934. On the regenerative power of the uterus. J Anat 69(pt 1):79–81, PMID: 17104518.

Sferruzzi-Perri AN, Camm EJ. 2016. The programming power of the placenta. Front Physiol 7:33, PMID: 27014074, https://doi.org/10.3389/fphys.2016.00033.

Shao Y, Guan Y, Wang L, Qiu Z, Liu M, Chen Y, et al. 2014. CRISPR/Cas-mediated genome editing in the rat via direct injection of one-cell embryos. Nat Protoc 9(10):2493–2512, PMID: 25255092, https://doi.org/10.1038/nprot.2014.171.

Shenoy V, Kanasaki K, Kalluri R. 2010. Pre-eclampsia: connecting angiogenic and metabolic pathways. Trends Endocrinol Metab 21(9):529–536, PMID: 20646932, https://doi.org/10.1016/j.tem.2010.05.002.

Soares MJ, Chakraborty D, Karim Rumi MA, Konno T, Renaud SJ. 2012. Rat placentation: an experimental model for investigating the hemochorial maternal-fetal interface. Placenta 33(4):233–243, PMID: 22284666, https://doi.org/10.1016/j.placenta.2011.11.026.

Soares MJ, Chakraborty D, Kubota K, Renaud SJ, Rumi MAK. 2014. Adaptive mechanisms controlling uterine spiral artery remodeling during the establishment of pregnancy. Int J Dev Biol 58(2–4):247–259, PMID: 25023691, https://doi.org/10.1387/ijdb.140083ms.

Soares MJ, Iqbal K, Kozai K. 2017. Hypoxia and placental development. Birth Defects Res 109(17):1309–1329, PMID: 29105383, https://doi.org/10.1002/bdr2.1135.

Soares MJ, Varberg KM, Iqbal K. 2018. Hemochorial placentation: development, function, and adaptations. Biol Reprod 99(1):196–211, PMID: 29481584, https://doi.org/10.1093/biolre/ioy049.

Stegeman JJ, Hahn ME, Weisbrod R, Woodin BR, Joy JS, Najibi S, et al. 1995. Induction of cytochrome P4501A1 by aryl hydrocarbon receptor agonists in porcine aorta endothelial cells in culture and cytochrome P4501A1 activity in intact cells. Mol Pharmacol 47(2):296–306, PMID: 7870038.

Stejskalova L, Pavek P. 2011. The function of cytochrome P450 1A1 enzyme (CYP1A1) and aryl hydrocarbon receptor (AhR) in the placenta. Curr Pharm Biotechnol 12(5):715–730, PMID: 21342125, https://doi.org/10.2174/138920111795470994.

Stejskalova L, Vecerova L, Peréz LM, Vrzal R, Dvorak Z, Nachtigal P, et al. 2011. Aryl hydrocarbon receptor and aryl hydrocarbon nuclear translocator expression in human and rat placentas and transcription activity in human trophoblast cultures. Toxicol Sci 123(1):26–36, PMID: 21666223, https://doi.org/10.1093/toxsci/kfr150.

Stuart T, Butler A, Hoffman P, Hafemeister C, Papalexi E, Mauck WM III, et al. 2019. Comprehensive integration of single-cell data. Cell 177(7):1888–1902.e21, PMID: 31178118, https://doi.org/10.1016/j.cell.2019.05.031.

Sturtzel C. 2017. Endothelial cells. Adv Exp Med Biol 1003:71–91, PMID: 28667554, https://doi.org/10.1007/978-3-319-57613-8_4.

Thackaberry EA, Jiang Z, Johnson CD, Ramos KS, Walker MK. 2005. Toxicogenomic profile of 2,3,7,8-tetrachlorodibenzo-*p*-dioxin in the murine fetal heart: modulation of cell cycle and extracellular matrix genes. Toxicol Sci 88(1):231–241, PMID: 16120747, https://doi.org/10.1093/toxsci/kfi301.

Tsuchiya Y, Nakajima M, Yokoi T. 2005. Cytochrome P450-mediated metabolism of estrogens and its regulation in human. Cancer Lett 227(2):115–124, PMID: 16112414, https://doi.org/10.1016/j.canlet.2004.10.007.

Vaughan OR, Sferruzzi-Perri AN, Coan PM, Fowden AL. 2011. Environmental regulation of placental phenotype: implications for fetal growth. Reprod Fertil Dev 24(1):80–96, PMID: 22394720, https://doi.org/10.1071/RD11909.

Wakeland AK, Soncin F, Moretto-Zita M, Chang C-W, Horii M, Pizzo D, et al. 2017. Hypoxia directs human extravillous trophoblast differentiation in a hypoxia-inducible factor-dependent manner. Am J Pathol 187(4):767–780, PMID: 28167044, https://doi.org/10.1016/j.ajpath.2016.11.018.

Watson JD, Prokopec SD, Smith AB, Okey AB, Pohjanvirta R, Boutros PC. 2014. TCDD dysregulation of 13 AHR-target genes in rat liver. Toxicol Appl Pharmacol 274(3):445–454, PMID: 24355419, https://doi.org/10.1016/j.taap.2013.12.004.

Wesselink A, Warner M, Samuels S, Parigi A, Brambilla P, Mocarelli P, et al. 2014. Maternal dioxin exposure and pregnancy outcomes over 30 years of follow-up in Seveso. Environ Int 63:143–148, PMID: 24291766, https://doi.org/10.1016/j.envint.2013.11.005.

Wettschureck N, Strilic B, Offermanns S. 2019. Passing the vascular barrier: endothelial signaling processes controlling extravasation. Physiol Rev 99(3):1467–1525, PMID: 31140373, https://doi.org/10.1152/physrev.00037.2018.

Whitlock JP Jr. 1999. Induction of cytochrome P4501A1. Annu Rev Pharmacol Toxicol 39:103–125, PMID: 10331078, https://doi.org/10.1146/annurev.pharmtox.39.1.103.

Wiemers DO, Ain R, Ohboshi S, Soares MJ. 2003. Migratory trophoblast cells express a newly identified member of the prolactin gene family. J Endocrinol 179(3):335–346, PMID: 14656203, https://doi.org/10.1677/joe.0.1790335.

Wilson CL, Safe S. 1998. Mechanisms of ligand-induced aryl hydrocarbon receptor-mediated biochemical and toxic responses. Toxicol Pathol 26(5):657–671, PMID: 9789953, https://doi.org/10.1177/019262339802600510.

Wright EJ, De Castro KP, Joshi AD, Elferink CJ. 2017. Canonical and non-canonical aryl hydrocarbon receptor signaling pathways. Curr Opin Toxicol 2:87–92, PMID: 32296737, https://doi.org/10.1016/j.cotox.2017.01.001.

Wu Y, Chen X, Zhou Q, He Q, Kang J, Zheng J, et al. 2014. ITE and TCDD differentially regulate the vascular remodeling of rat placenta via the activation of AhR. PLoS One 9(1):e86549, PMID: 24475139, https://doi.org/10.1371/journal.pone.0086549.